INTERFACE

royalsocietypublishing.org/journal/rsif

Review

Cite this article: Gao X, Fraulob M, Haïat G. 2019 Biomechanical behaviours of the bone–implant interface: a review. *J. R. Soc. Interface* **16**: 20190259.
http://dx.doi.org/10.1098/rsif.2019.0259

Received: 8 April 2019
Accepted: 1 July 2019

Subject Category:
Life Sciences–Engineering interface

Subject Areas:
biomedical engineering, biomechanics, medical physics

Keywords:
biomechanical behaviour, bone–implant interface, mechanical measurement, stability, cementless

Author for correspondence:
Guillaume Haïat
e-mail: guillaume.haiat@univ-paris-est.fr

Biomechanical behaviours of the bone–implant interface: a review

Xing Gao[1,2], Manon Fraulob[1] and Guillaume Haïat[1]

[1]CNRS, Laboratoire Modélisation et Simulation Multi Echelle, UMR CNRS 8208, 61 avenue du Général de Gaulle, 94010 Créteil cedex, France
[2]Research Centre for Medical Robotics and Minimally Invasive Surgical Devices, Shenzhen Institutes of Advanced Technology, Chinese Academy of Sciences, Shenzhen 518055, People's Republic of China

In recent decades, cementless implants have been widely used in clinical practice to replace missing organs, to replace damaged or missing bone tissue or to restore joint functionality. However, there remain risks of failure which may have dramatic consequences. The success of an implant depends on its stability, which is determined by the biomechanical properties of the bone–implant interface (BII). The aim of this review article is to provide more insight on the current state of the art concerning the evolution of the biomechanical properties of the BII as a function of the implant's environment. The main characteristics of the BII and the determinants of implant stability are first introduced. Then, the different mechanical methods that have been employed to derive the macroscopic properties of the BII will be described. The experimental multi-modality approaches used to determine the microscopic biomechanical properties of periprosthetic newly formed bone tissue are also reviewed. Eventually, the influence of the implant's properties, in terms of both surface properties and biomaterials, is investigated. A better understanding of the phenomena occurring at the BII will lead to (i) medical devices that help surgeons to determine an implant's stability and (ii) an improvement in the quality of implants.

1. Introduction

Population ageing and the occurrence of road traffic, sports and work accidents are the main reasons for the increasing interest of the research community in studying the osteoarticular system. Implanting biomaterials within bone tissue to restore the functionality of the treated organ has become a common technique in orthopaedic and dental surgery [1]. Implants and articular prostheses have led to important progress in the repair of joint degeneration (hip, knee…) and in maxillofacial surgery (to restore missing teeth or support craniofacial reconstructions). Modern orthopaedic and dental implant treatments aim at a rapid, strong and long-lasting attachment between implant and bone tissue.

Despite their routine clinical use, implant failures still occur and remain difficult to anticipate as the reasons for implant losses remain unclear. The surgical success of implant surgeries depends on the evolution of the biomechanical properties of the bone–implant interface (BII), which remains difficult to determine *in vivo*. Predicting implant failure is difficult because bone is a complex multi-scale medium evolving as a function of time through remodelling phenomena. Moreover, the presence of an interface complicates the situation. Another difficulty arises from the fact that the implant's success depends on multi-factorial aspects related to the patients (e.g. behaviour, bone quality), to the surgeons (e.g. aseptic conditions during surgery, surgical and loading protocol) and to the implant manufacturers (e.g. implant surface, biomaterial, implant geometry).

Bone is a strong and lightweight composite multi-scale anisotropic material which presents a hierarchy of microstructures [2]. At the scale of several hundred nanometres, mineralized bone is composed of elementary components such as hydroxyapatite, cylindrically shaped collagen molecules and water. At the scale of 1–10 µm, bone is constituted by the ultrastructure, which is composed of collagen fibres and extrafibrillar spaces. At the scale of several

THE ROYAL SOCIETY PUBLISHING

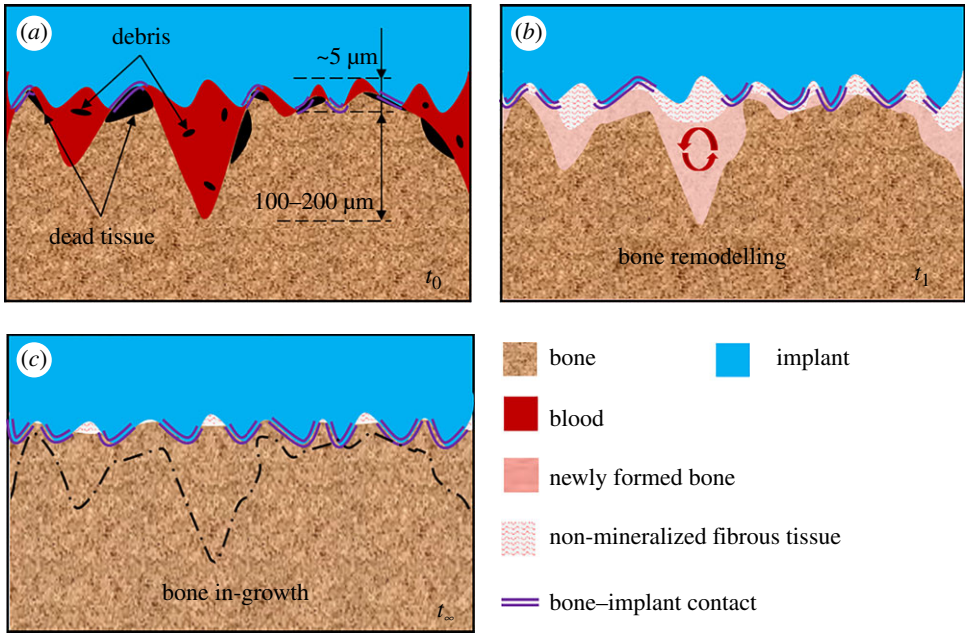

Figure 1. Schematic of the bone–implant interface (*a*) immediately after surgery (time t_0), (*b*) during the bone remodelling period t_1 (formation of newly formed bone) and (*c*) after completion of osseointegration t_∞. (Online version in colour.)

hundred micrometres to several millimetres, the microstructure depends on the type of bone.

Besides its multi-scale nature, bone can adapt its structure through remodelling phenomena [3], which induce changes in its structure and mechanical properties to accommodate the presence of an implant. A better understanding of the biomechanical properties of newly formed bone around the implant interface may lead to more accurate prediction of the surgical outcome of implant integration [4], preventing additional painful and expensive surgical interventions.

Implant retention is determined by interfacial phenomena such as friction or mechanical interlocking. Surface roughness influences its mechanical stability [5]. Rough surface structures may stimulate the repair of bone tissue [6] and may also introduce mechanically based effects in bone, such as interlocking due to bone growth into the surface [7].

Despite the aforementioned difficulties, the industrial design of implants has often been driven by an aggressive 'copycat' marketing approach rather than by fundamental advances in biomechanics [8]. Clinicians have often used implants in new applications before research has been carried out from a basic science viewpoint. Empirical approaches are limited to understanding the interaction of the mechanisms determining osseointegration phenomena.

To date, cemented and cementless implants are the two main types of implants used in orthopaedic surgery, while, to the best of our knowledge, bone cement is not used for the anchorage of oral implants. Although bone cement, acting as a bonding medium, can provide initial fixation, cementless implants are now more and more often preferred because of the risks of cemented implant failures related to an accumulation of micro-cracks in and around the cemented area [9]. Moreover, systemic risks such as cement implantation syndrome during and after the cementation procedure have been noticed [10]. Consequently, this work focused only on cementless implants where bone tissue is in direct contact with the implant surface.

The aim of this review is to provide the state of the art on the evolution, the measurement and the dependence of the biomechanical properties of the BII, which is important because (i) it is related to the primary and secondary stability of the implant and (ii) the BII is suggested to be the weakest domain in the bone–implant system and is where most failures occur [11].

In this review, we chose to focus on aspects related to biomechanics. Readers interested in biological or biochemical aspects are referred to other publications, for example [12–18]. An introduction to the evolution of the biomechanical properties of the BII and its relation to implant stability will be given in §2. Then, various methods used to assess the biomechanical properties of the BII at the macroscopic scale will be described, such as mechanical tests with tensile, shear, torque and friction tests. Then, different experimental techniques aimed at determining the microscopic biomechanical properties of newly formed bone tissue will be investigated. Eventually, the influence of the environment such as the type of biomaterial and the surface roughness on the biomechanical properties of the BII will be investigated.

2. Implant stability

The biomechanical properties of the BII are the determinant for implant stability. A good quality of bone healing leads to: (i) direct contact between mineralized bone tissue and the implant and (ii) an important proportion of the implant surface in intimate contact with bone tissue. The success of implant surgery is determined by the biomechanical quality of bone tissue located at a distance less than around 100–200 µm from the implant surface [19,20]. The quantity is also an important parameter for surgical success, even if Bolind *et al.* [21] reported that the bone–implant contact ratio (BIC) in successful oral implants varied between 60% and 99% with no evidence whatsoever that those implants with 99% BIC fared any better than those that have BIC values of 60%. The BIC ratio is correlated with the biomechanical properties of the BII and increases during bone healing [20,22], as first described by Johansson and Albrektsson in 1987 [23].

Figure 1 describes schematically the evolution of the BII as a function of healing time, known as *osseointegration*

phenomena, which were first defined by Brånemark in 1977 [24]. Just after surgery (figure 1*a*), the implant surface is surrounded by blood (due to the reaming of the bone cavity) as well as dead and living bone tissue. Bone debris may also be present around the implant surface. During bone healing, which occurs several weeks/months after surgery, newly formed bone is produced to fill the gap between mature bone tissue and the implant surface (figure 1*b*). Several weeks or months after the implant surgery, newly formed bone tissue is replaced progressively by mature bone tissue around the implant surface, leading to the final BIC ratio as shown in figure 1*c*.

Histological analysis is the gold standard to determine the BIC but it cannot be used in clinical practice. Classical X-ray-based techniques [25] and magnetic resonance imaging [26] cannot be used to assess the BIC because of metal artefacts related to the presence of titanium [25].

2.1. Primary stability of cementless implant

Cementless implants can be either screwed home in bone tissue (which is the case for dental implants and some orthopaedic implants) or inserted in bone tissue using the 'press-fit' technique (for orthopaedic implants), which consists in introducing the implant into a cavity (slightly smaller than the implant size) formed by drilling or cutting, thus leading to the primary stability of the implant through the pre-stressed state of the bone tissue [27–29]. Frictional properties of the BII are then the determinant to ensure a proper implant stability at early post-operative stages (see §3.2). Primary stability is defined as the stability of the implant just after surgical insertion, before the healing period.

Friction phenomena between the implant surface and bone tissue are used to sustain shear load at the BII [30] (e.g. at the tibia [31], hip [32], femur [33], glenoid [34]). Screwing may also be important to provide mechanical fixation (e.g. dental [19], spinal devices [35], intramedullary rods [36]). Although surgery may damage bone tissue, it also triggers a cascade of wound-healing events that stimulate osseointegration, a biological process improving implant stability through bone remodelling.

Insufficient primary stability leads to excessive interfacial micromotion following surgery [37,38], which may imply a higher occurrence of migration [39] and of implant failure. Early post-operative migration was suggested to be correlated with long-term loosening after around 8 years [40], emphasizing a crucial role of primary stability of cementless implants in the fate of implant survival. Furthermore, the primary stability should not be too high since an excessive level of stresses (the precise amplitude of which remains to be quantified) may lead to bone necrosis [41,42].

2.2. Osseointegration and secondary stability

During the post-operative period, bone adapts its structure to the mechanical stresses it undergoes through remodelling phenomena [3], which induces changes in bone properties to accommodate its structure to the presence of the implant. Bone formation relies on complex signalling pathways sensitive to biomechanical stimulation, which remain unclear, and is achieved through intramembranous ossification and osteoblast activation. Bone regeneration after implantation lasts several months, during which the spatio-temporal evolution of the bone properties are highly heterogeneous. The main steps of bone regeneration are: (i) the deposition of an extracellular matrix or osteoid tissue, an unmineralized collagen-rich tissue, (ii) mineralization of the osteoid by hormonal stimulation of local calcium and phosphate ions to form woven bone (a disordered mineralized tissue), and (iii) remodelling of woven bone to mature bone.

At the macroscopic scale, empirical models have mostly been employed using *ad hoc* assumptions deriving from Wolff's law [43]. At the nanometre scale, the process of bone formation is affected by local features such as fluid and chemical pathways as well as the stress state [44]. Models of bone remodelling should account for the flow channels which provide conduits for fluid flow, enhancing molecular and cellular transport and inducing shear stresses via fluid drag at the cell surfaces, an essential condition for cell survival [45,46]. In particular, fluid flow occurs in the canaliculi [47,48], which are small channels (diameter between 100 nm and 1 µm [49–51]). Since bone pore walls present a negative surface charge, coupling effects with ions contained in interstitial fluid may appear [52]. Electrical phenomena have been observed in bone since the 1950s, but their physiological origin is still debated [53,54]. Methods based on continuum mechanics may not be suited to dealing with fluid transport in nanopores, where it is crucial to consider an atomic-level description of the interactions occurring at the interface between the hydroxyapatite and the fluid [55]. Surface effects are likely to play a key role in transport phenomena at the nanoscale in pores with a size not much larger than the molecular size, where hydration and steric effects may induce changes in the fluid properties. One of the main challenges now consists in coupling multi-scale models with temporal bone evolution due to remodelling phenomena [56].

Osseointegration and mature bone in-growth around dental implants allows the quantity of bone in contact with the implant to be improved as well as bone quality surrounding the implant [57], thus promoting mechanical interlocking [58]. Therefore, the impact of osseointegration phenomena is to strengthen the secondary stability of the implant, which is a function of healing time. During the early period of healing time (one to three weeks), a decrease in secondary stability has been described for dental implants, which may be due to osteoclast activity [19].

However, the situation is not so clear regarding orthopaedic impant osseointegration. The term osseointegration indicates a direct and microscopic contact between bone tissue and the implant surface. In orthopaedic surgery, there is little evidence that cementless implants are actually osseointegrated. Some authors evidenced a fibrous tissue interface [59] at the BII of orthopaedic implants. The reason for hip and knee replacements demonstrating distance osteogenesis is not known but may be related to either the use of certain metals or to the blunt surgery performed with reaming of the marrow cavity and hammering in the implant that shows some micromotion during the first few months after implant placement. However, orthopaedic, cementless implants definitely have a good clinical outcome, indicating that they show adequate stability probably related to the osteogenesis occurring at distance from the implant surface.

During bone healing, low-amplitude micromotions stimulate bone remodelling [60], but fibrous tissues may develop instead of an osseointegrated interface in the case of excessive interfacial micromotion following surgery [37], in particular for dental implants. Experimental results

showed that micromotion lower than 40–70 µm allows bone tissue in-growth [61]. However, an excessive level (typically above 150 µm) results in the formation of peri-prosthetic fibrous tissue instead of an osseointegrated interface [61–63]. Note that fibrous tissue has a stiffness of around 0.5–2.0 kPa [64], which is several orders of magnitude less rigid than both mature and newly formed bone tissue at the BII. The presence of fibrous tissue therefore affects the load-bearing capacity of the implant and leads to a vicious circle (since micromotions are further enhanced) responsible for implant failures. Moreover, fibrous connective tissue can form in the long term owing to release of wear particles from the implant-bearing surface [65,66], in particular in orthopaedic surgery.

Resonant frequency analysis (RFA) has become a widely used method to determine the secondary stability of dental implants [67]. RFA is a non-invasive technique used to assess *in vivo* dental implant stability by measuring the variation in stiffness of the bone–implant system [68,69], which is presented by an implant stability quotient (ISQ) value. High ISQ values are synonymous with important implant stability [70]. Readers are referred to other reviews [19,71,72] for more details on the RFA technique, which is outside the scope of the present study.

3. Macroscopic testing of the bone–implant interface

Various types of biomechanical testing employing different loading conditions have been introduced in order to measure the biomechanical properties of the BII. Some authors have considered implants actually used in the clinic (see §3.1) while others have employed custom-made implants with a simplified geometry and loading conditions, which enables the implants to be studied under standardized conditions. Initial mechanical fixation in the immediate post-operative period t_0 (figure 1*a*) will be studied in §3.2, including the frictional behaviour of the BII. The evolution of the biomechanical properties of the BII during osseointegration will then be investigated using various approaches in §3.3.

3.1. Using implants employed in the clinic

Many studies in the dental and orthopaedic fields have been carried out using implants employed in clinical practice. Two different testing configurations can be distinguished. The first one consists in an estimation of the micromotion at the BII while the second one consists in realizing the macroscopic pull-out tests.

3.1.1. Micromotion measurement

An 'excessive' level of micromotion at the BII limits the chances of implant success, which explains why different groups have measured micromotions through the application of cyclic stresses onto the implant. Such an approach has been carried out by implant manufacturers to validate the design of new implants [73,74]. Although the threshold above which osseointegration fails depends on the patient, a micromotion level above 150 µm is commonly accepted to possibly induce implant failure [61–63].

Various studies have evaluated micromotion obtained under physiological loading during a patient's daily activities [38], which was often determined through gait analysis by marker clusters and instrumented implants with sensors such as strain gauges [75–78]. Various angles were determined for the loading direction relative to the implant axis, which led to a combination of axial, bending and torsional loading conditions allowing *in vivo* loading conditions to be mimicked [79].

Advanced image-processing techniques such as micro-extensiometry [73] and digital image correlation [80,81] have been employed to increase the sensitivity of the technique. However, although post-mortem studies may be carried out to analyse the BII [82], one important limitation for *in vivo* practices lies in the fact that the BII cannot be directly observed, thus limiting the measurement accuracy. An advanced micro-computed tomography (µCT)-based technique was developed to measure relative micromotions between markers located at the implant surface and markers fixed in the surrounding bone, allowing the primary stability of the femoral stem to be assessed [33]. Using a linear variable differential transducer (LVDT) is another technique to measure micromotion at the BII and to evaluate femoral stem primary stability. These devices are fixed in holes drilled at the bone surface, allowing contact with the prosthesis to measure micromotions between the two components at locations of interest [83–87]. However, such methods cannot be implemented in the operating room because of metal artefacts due to metal implants for the µCT-based technique and the unphysiological aspect of LVDTs.

Micromotion values obtained experimentally have been compared with numerical models. For instance, a three-dimensional finite-element model was developed to predict the interfacial micromotion of a cementless knee–tibia prosthesis and to assess the risk of aseptic loosening. The numerical results were compared with experimental measurements under walking and stair-climbing loading [31]. Similar approaches have been carried out for femoral stem implants [88–91].

3.1.2. Pull-out tests

The measurement of the maximum pull-out force is another parameter that has been used to estimate implant stability [90], because the pull-out force is directly related to implant loosening [92]. Many studies have been carried out using such an approach for various types of implants, such as hip [93] and knee [92] implants (in cadaveric studies) or dental implants [94]. However, a strong limitation of such an approach lies in that the crack propagates in an unstable manner at the BII, which prevents investigation of the interface mechanical strength.

3.2. Dedicated implant models to measure initial mechanical fixation

All implants employed in clinical practice have a complex geometry, which leads to spatially complex, non-uniform, multi-axial stress fields [95] when the implant is loaded. This heterogeneous stress distribution involving compressive and shear stress components may influence the results obtained in such a configuration [94], and it is therefore difficult to analyse the results in order to estimate a physically meaningful value for the interfacial mechanical strength. This is the reason why dedicated implant models have been developed, since mechanical parameters can be experimentally determined under a controlled and standardized situation, allowing them to be studied under simpler conditions. Such implants are considered in this subsection.

The frictional behaviour at the BII provides initial mechanical fixation for the implant's primary stability. Assessing the friction coefficient is important to understand the behaviour of the BII during and just after surgery and thus to

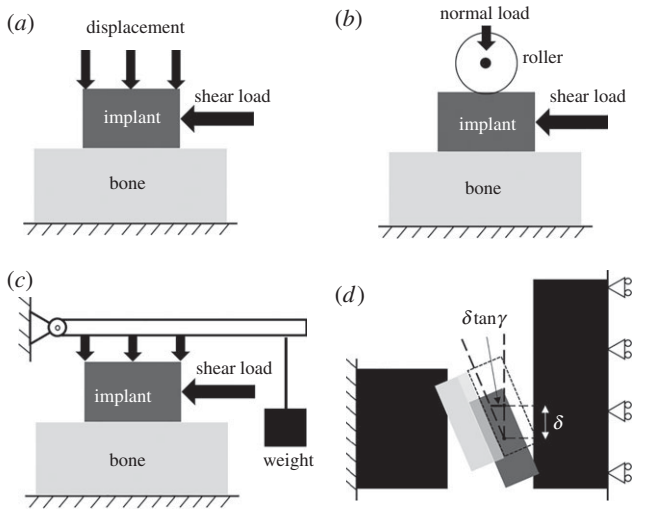

Figure 2. Schematic description of different experimental configurations dedicated to the measurement of the frictional behaviour of the bone–implant interface. (*a*) Applied normal pressure, (*b*) applied normal load with a loading direction perpendicular to the bone–implant interface, (*c*) constant normal pressure applied using a weight and (*d*) simplified press-fit test accounting for the interference fit.

prevent micromotion at the BII, which may cause implant failure. Moreover, the frictional behaviour is an important input parameter to be used in finite-element models [96,97] in order to model implant surgical procedures.

The most common experimental configuration to measure the friction coefficient is to apply a displacement of the implant perpendicularly to the BII and to induce sliding by moving one domain relative to the other one in the plane of the interface (figure 2*a*). Rancourt *et al*. [98] carried out a seminal work in this domain and evidenced a nonlinear friction behaviour at the initial stage prior to complete sliding, which corresponds to a nonlinear variation in the tangential force as a function of the displacement. The nonlinear behaviour could be defined by a gradual process—complete stiction, partial stiction and partial sliding, complete sliding—as described in [99]. It was also evidenced that the friction coefficient was independent of the applied normal force [30,98,100] and displacement rate [98], but depends on the properties of the bone tissue surrounding the implant [100] and on the properties of the implant surface [30,98,100]. However, further work is needed in order to investigate the dependence of the nonlinear variation of the tangential force as a function of the displacement (i.e. for low values of displacement).

Biemond *et al*. [58] considered an alternative experimental configuration by placing a roller on top of the implant, which is used to apply a load perpendicularly to the implant surface (figure 2*b*). Another testing configuration was developed by Grant *et al*. [101], who considered the application of the normal force using a constant weight (figure 2*c*), which may not occur using a testing machine under load-controled regimes because of possible issues related to the sensitivity of force feedback system [73]. To the best of the authors' knowledge, no study coupled a roller and weight-load to minimize errors in the friction coefficient measurement, which results from variation in the normal force and mismatch between the loading direction and the normal direction of the contact surface.

Other studies [27,92] implemented realistic configurations to investigate the dependence of the maximum pull-out force after fully inserting implants into bone cavities. For instance, cylindrical-shaped implants with various surface roughness were inserted into bone cavities slightly smaller than the implant size (the difference between the diameters of the implant and of the cavity is called the interference fit). The pull-out forces were then measured, thus allowing the relation between the interference fit and implant primary stability to be investigated [27]. The results demonstrated that a larger interference fit leads to higher values of the pull-out force. While non-osseointegrated implants (i.e. in the absence of any healing) with rough surfaces are expected to lead to higher pull-out force due to higher friction, the opposite behaviour was obtained in [27], which could stem from bone damage, wear and bone debris generated during the insertion and acting as lubrication. The impact of the interference fit can also be studied with finite-element models as in [102,103], where the results were compared with experimental data.

Another testing configuration was developed by Bishop and colleagues [104–106] in a series of papers modelling the press-fit configuration (figure 2*d*) and taking into account the effect of the interference fit. They considered two parallelepiped specimens for the bone sample and for the implant. This testing configuration allows the measurement of radial loading, which is important to understand bone deformation and damage during press-fitting. Two methods were developed—force and displacement controlled modes—to model the primary stability of press-fitted implants. The pull-out force was used as a surrogate of the implant primary stability in order to compare the effect of various loading conditions and implant surface properties on primary stability. Bone damage was characterized by analysing the structural change of the bone surface. In the tested configuration, the implant primary stability was shown to depend on the press-fit-related stress and to be independent of the roughness of the implant surface and of bone density [105,106]. Moreover, the friction coefficient was found to be related to normal stress for a porous-surface implant, especially for high stress level [104].

Table 1 summarizes the results found in the literature for different values of the friction coefficients of the BII with various types of biomaterials, surface properties, testing configurations and normal forces. Based on the documented values in table 1, two conclusions can be drawn. First, bovine trabecular bone with higher porosity than bovine cortical bone leads to a higher friction coefficient [107]. Second, higher surface roughness leads to a higher value of the friction coefficient [101,104]. In particular, the values of the friction coefficient obtained in human cortical bone [58] seem higher than the values obtained in human trabecular bone [101]. However, the results in cortical bone [58] were obtained at 37°C in water, which is not the case of those obtained in trabecular bone. The hydration state is likely to have a significant effect on the frictional behaviour of the BII. Moreover, the surface roughness of the Ti implant used in [58] was not provided. Most measurements were realized with relatively low normal stresses (less than 1 MPa), thus leading to a weak dependence of the frictional behaviour on the normal force.

3.3. Variation of the biomechanical properties of the bone–implant interface during healing

3.3.1. Shear and tensile test

The properties of the BII during healing have been measured using push-out and pull-out tests (figure 3*a*,*b*). An example

Table 1. Summary of the results found in the literature for the friction coefficients of implants with various types of biomaterials, surface properties, testing configurations and normal forces.

	implant materials		implant surface characteristics		testing condition					
	materials	surface treatment	roughness R_a (µm)	porosity (%)	temp.	ambience	testing configuration	normal stress/force (MPa)	friction coefficient	ref.
human trabecular bone	titanium	polish	0.11	—	room temp.	air	cyclic dynamic sliding in sinusoidal pattern	0.25, 0.5 and 1	0.37 ± 0.02	[101]
		Al_2O_3-blast	11.00						0.48 ± 0.06	
		plasma-spray	19.00						0.45 ± 0.03	
		beaded porous	32.60						0.42 ± 0.01	
human trabecular bone	titanium	polish	0.11	0	room temp.	air	simplified interference fit	peak magnitudes of 5.6–11.7	0.16 ± 0.05	[104]
		beaded porous	32.6	45					0.86 ± 0,02	
		flaked porous	133	63					1.08 ± 0.04	
human trabecular bone	—	beaded porous	—	—	room temp.	air	sliding	0.1, 0.15 and 0.25	0.68 ± 0.10	[100]
	Co-Cr alloy	nonplanar mesh							0.75 ± 0.12	
		cast mesh type I							0.66 ± 0.09	
		cast mesh type II							0.94 ± 0.14	
human trabecular bone	titanium	beaded porous	—	—	room temp.	air	sliding	0.1–0.4	0.53 ± 0.07	[98]
		fibre meshed							0.47 ± 0.03	
	stainless steel	smooth							0.30 ± 0.02	
human trabecular bone	titanium	fibre meshed	—	35–45	room temp.	air	sliding	0.1, 0.15 and 0.25	0.63 ± 0.01	[30]
		beaded porous (Zimmer)		40–70					0.62 ± 0.02	
		beaded porous (Vitallium)		30–40					0.53 ± 0.02	
	stainless steel	smooth		0					0.43 ± 0.01	
bovine trabecular bone	porous tantalum	net-shape formed	—	—	room temp.	air	sliding	—	0.98 ± 0.17	[107]
		electron-discharge-machine formed							0.88 ± 0.09	
bovine cortical bone		net-shape formed							0.82 ± 0.15	
		electron-discharge-machine formed							0.74 ± 0.07	
bovine trabecular bone	—	OsteoAnchor	—	—	room temp.	air	unidirectional rotation	0.57 and 0.85	1.04 ± 0.18	[73]
	tantalum	porous							0.95 ± 0.05	
	titanium	plasma-spray							0.55 ± 0.05	
human cortical bone	Ti6Al4V	E-beam wave pattern	—	—	37°C	water	sliding	40 N	0.68 ± 0.04	[58]
		E-beam cubic pattern							0.63 ± 0.03	
	titanium	plasma-spray							0.64 ± 0.04	
		sandblasted							0.49 ± 0.06	

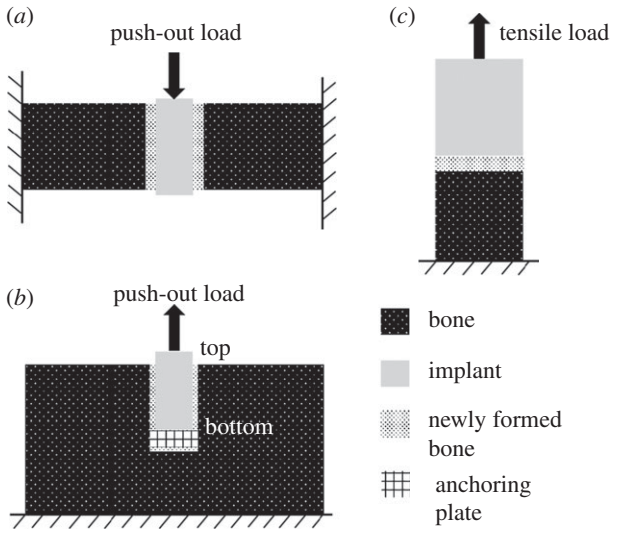

Figure 3. Schematic of (*a*) push-out test, (*b*) pull-out test and (*c*) tensile test.

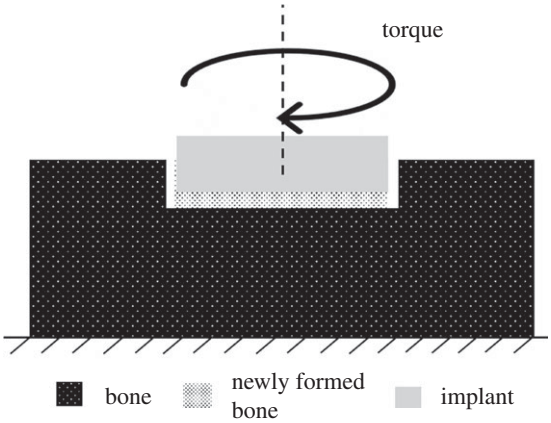

Figure 4. Schematic of torque tests with the configuration of the coin-shaped implant [117].

can be found in Castellani *et al*. [108] and Tschegg *et al*. [109], who measured the stiffness and the energy necessary to detach the implant, which was given by the area under the load–displacement curves [108,109]. However, the results are highly dependent on crack initiation since the crack propagates in an unstable manner, which prevents useful information on the effective adhesion energy of the BII being retrieved. Another experimental pull-out configuration consisted in using cylindrical implants in combination with an anchoring plate (figure 3*b*) [110]. The anchoring plate was used to isolate the bottom surface of the implant from bone tissue, ensuring that no stress was applied to this bottom surface during the pull-out phase. Another study also considered cylindrical implants under push-out tests [111], where the BII shear modulus was defined by the slope of the stress/strain unloading curve.

Although the pull-out and push-out tests described above may be qualitatively informative on the biomechanical properties of the BII, strong limitations apply, such as (i) misalignment errors [112,113] and (ii) possible migration of the implant within bone tissue during bone healing. Another (and maybe more important) limitation lies in the fact that cracks propagate in an unstable manner at the BII in mode II (which corresponds to the application of a shear stress applied in the plane of the interface and to a crack propagation in the direction of the principal plane of solicitation), making it difficult to determine the effective adhesion energy of the BII. When the crack propagates in an unstable manner, the only parameter affecting the macroscopic variable is given by crack initiation and it is then impossible to measure the effective adhesion energy due to the instability of the configuration. Therefore, stable mechanical testing configurations are needed to assess the mechanical strength of the BII. Debonding of the interface depends on a coupling of friction and adhesion phenomena at the BII [108,109]. Implant retention can be generally regarded as a combined result of friction, mechanical interlocking and chemical bonding [114], which makes it difficult to clearly distinguish between the different effects using such a testing configuration.

Therefore, tensile tests in the direction perpendicular to the implant surface have been developed in order to minimize the effect of mechanical interlocking, thus involving mostly adhesive fracture (mode I, which corresponds to the application of a tensile stress applied to the interface) between bone and implant [115,116] (figure 4). Ronold and colleagues [22,114,118–120] established an animal model involving the use of a flat coin-shaped implant placed onto cortical bone of a rabbit tibia without mechanical fixation. During the healing period, the contact between the coin-shaped implant and bone tissue was restricted to the flat surface owing to the presence of polytetrafluoroethylene (PTFE). After the animal was sacrificed, the implant was subjected to a quasi-static tensile-loading regime, and the effects of surface roughness [118], surface treament [120] and healing time [119] on the pull-out force was investigated. The results are summarized in table 2. However, similar to the configurations described in figure 3*a*, *b*, the crack propagation occurs in an unstable manner [108,109] because this pull-out test corresponds to an unstable flat-punch configuration [122]. This situation makes it difficult to determine the effective adhesion energy (or the strain energy release rate), which is the only physically meaningful parameter to investigate the bone–implant attachment, because the measured pull-out force depends on the initial contact conditions, in particular around the implant surface. These limitations constitute further motivations to develop alternative approaches such as the torque test configurations described below and introduced in [23].

3.3.2. Torque test

Torque tests to evaluate osseointegrated implants were initially introduced by Johansson and Albrektsson [23], who started performing manual measurements and then developed automated torque tests [123]. However, from a biomechanical perspective, implant threading complicates the geometrical configuration, making it challenging to retrieve meaningful parameters from a mechanical point of view. For this reason, a specific implant model having a planar BII and deriving from the seminal papers of Ronold *et al*. [22,114,118–120] was developed by our group. Employing a torque test applied to a coin-shaped implant model constitutes a powerful approach to obtaining steady-state crack propagation at the BII, as shown in figure 4. Moreover, mode III (which corresponds to the application of a shear stress applied in the plane of the interface and to a crack propagation in the direction perpendicular to the principal plane of solicitation) is likely to occur *in vivo*, in particular in the case of orthopaedic implants, which undergo multi-axial stress fields during daily living activity. In this

Table 2. Summary of the macroscopic biomechanical properties of BII by tension, shear and torsion tests in the literature.

animal model			implant				biomechanical properties of BII			
animal	contact tissue	healing period	material	surface treatment (particle size)	surface roughness (R_a, μm)	testing configuration	stiffness (MPa)	strength (MPa)	fracture energy (Nm^{-1})	ref.
New Zealand rabbits	cortical bone	—	titanium	TiO_2 blasting	1.43 ± n.a.	coin-shaped tension	—	0.11 ± 0.05	—	[114]
		2 weeks		TiO_2 blasting (180–220 μm)	3.37 ± n.a.			0.02 ± 0.04		[119]
		4 weeks						0.20 ± 0.18		
		6 weeks						0.45 ± 0.30		
		8 weeks		TiO_2 blasting (22–28 μm)	1.12 ± 0.27			0.11 ± 0.03		[120]
				TiO_2 blasting (180–220 μm)	3.79 ± 1.07			0.84 ± 0.48		
				TiO_2 dual blasting (180–220/22–28 μm)	2.05 ± 0.20			0.16 ± 0.05		
				TiO_2 blasting (180–220 μm)	3.90 ± n.a.			0.53 ± 0.30		[118]
				TiO_2 blasting + acid etched (0.01 m HCl)	5.07 ± n.a.			0.35 ± 0.18		
				TiO_2 blasting + acid etched (1 m HCl)	11.03 ± n.a.			0.09 ± 0.02		
		10 weeks		TiO_2 blasting (22–28 μm)	1.25 ± 0.02			0.66 ± 0.37		[22]
				TiO_2 blasting (180–220 μm)	3.62 ± 0.56			1.78 ± 0.73		
				TiO_2 blasting (270–330 μm)	5.52 ± 0.74			1.53 ± 0.34		

(*Continued*.)

Table 2. (*Continued.*)

animal model			implant				biomechanical properties of BII			
animal	contact tissue	healing period	material	surface treatment (particle size)	surface roughness (R_a, µm)	testing configuration	stiffness (MPa)	strength (MPa)	fracture energy (Nm^{-1})	ref.
Sprague–Dawley rats	cortical and trabecular bone	4 weeks	titanium	—	0.60 ± 0.07	pull-out shear	—	1.02 ± 0.59	—	[108,109]
		12 weeks						4.36 ± 0.69		
		24 weeks						2.99 ± 1.62		
		4 weeks	PLGA polymer implant		—			0.98 ± 0.54		
		12 weeks						2.06 ± 0.59		
		24 weeks						1.52 ± 0.64		
		4 weeks	biodegradable magnesium alloy		0.76 ± 0.09			2.15 ± 0.59		
		12 weeks						6.75 ± 1.62		
		24 weeks						7.78 ± 1.76		
pigs	trabecular bone	3 weeks	titanium	grit blasting + high-temperature acid etching	—	pull-out shear	—	2.60 ± 1.49	—	[110]
				bio-functionalized P15/HA	—			5.84 ± 2.02		
New Zealand rabbits	cortical and trabecular bone	12 weeks	Ti6Al4V medical grade titanium alloy	Al_2O_3 blasting (500–710 µm)	7.25 ± n.a.	pull-out shear	36.53 ± 19.87	11.78 ± 5.77	—	[111]
				bulged cylindrical pores 100 µm	—		52.04 ± 40.06	8.39 ± 5.00		
				bulged cylindrical pores 200 µm			53.47 ± 18.86	9.07 ± 2.57		
				bulged cylindrical pores 300 µm			42.94 ± 10.92	7.85 ± 2.50		

(*Continued.*)

Table 2. (*Continued.*)

animal model			implant				biomechanical properties of BII			
animal	contact tissue	healing period	material	surface treatment (particle size)	surface roughness (R_a, µm)	testing configuration	stiffness (MPa)	strength (MPa)	fracture energy (Nm^{-1})	ref.
Merino wethers	cortical bone	4 weeks	Ti6Al4V medical grade titanium alloy	smooth	0.284 ± 0.002	push-in shear	—	—	—	[121]
		8 weeks						0.75 ± 0.52		
		12 weeks						0.90 ± 1.11		
		4 weeks		grit-blasted	5.68 ± 0.44			5.89 ± 3.33		
		8 weeks						7.59 ± 3.48		
		12 weeks						10.26 ± 3.11		
		4 weeks		grit-blasted + HA coated	6.57 ± 0.88			10.02 ± 6.07		
		8 weeks						16.32 ± 5.48		
		12 weeks						20.17 ± 6.52		
		4 weeks		sintered Ti beads	—			18.58 ± 10.44		
		8 weeks						31.62 ± 5.26		
		12 weeks						34.65 ± 5.33		
		4 weeks		sintered Ti beads + HA coated	—			17.39 ± 11.33		
		8 weeks						35.31 ± 6.37		
		12 weeks						39.97 ± 5.63		
New Zealand rabbits	cortical bone	7 weeks	Ti6Al4V medical grade titanium alloy	TiO_2 blasting	1.9 ± n.a.	coin-shaped torsion	240.00 ± 10.00	1.73 ± 0.08	77.5 ± 7.5	[117]

n.a., not applicable; PLGA, poly(lactic-co-glycolic acid).

testing configuration, the bone sample is attached to a rotation stage, while a torque sensor is linked to the implant. The crack propagates from the outer part of the planar interface towards the middle of the implant until complete debonding. The phenomena at work at the BII correspond to the coupling of friction and mode III crack propagation, a situation referred to as stiction [124]. An analytical model taking into account these phenomena was applied, leading to the determination of the effective fracture energy and the stress intensity factor [117]. The results are summarized in table 2.

4. Multi-scale characterization of newly formed bone tissue

As described in §2, the surgical outcome depends on the evolution of the biomechanical properties of the BII, which are given by the quantity and by the quality of bone tissue around the implant. Therefore, it is important to understand the evolution of the properties of newly formed bone tissue around the implant surface. Histomorphometry is the gold standard to assess osseointegration [125] and allows the BIC ratio to be measured. However, the quality and the biomechanical properties of periprosthetic bone tissue cannot be retrieved using histomorphometry. Moreover, histomorphometry is a destructive technique that cannot be used in clinical practice without having to carry out post-mortem experiments. Even if modelling and simulation allow powerful methods that take into account the effect of osseointegration at different scales to be implemented [31,126–129], an important advantage of applying multi-modality experimental techniques is that they allow complementary information on the multi-scale properties of newly formed bone tissue to be retrieved.

4.1. Nanoindentation and atomic force microscopy

Nanoindentation is one of the reference techniques used to retrieve the mechanical properties of a medium at the micro-scale [130,131]. A rigid indentation tip which has known properties and geometry (such as a Berkovich diamond three-sided pyramid probe [6,132]) is pressed into a material to retrieve the elastic modulus and hardness by analysing the curves representing the variation of the force as a function of the displacement, in particular at the beginning of the unloading phase using the Oliver and Pharr method [130]. Nanoindentation is an interesting technique to characterize periprosthetic tissue located near the BII because it allows the biomechanical properties of newly formed bone tissue to be studied. A study compared the elastic modulus and the hardness of newly formed bone tissue around a commercially pure titanium (cpTi) implant and a titanium–zirconium (TiZr1317) alloy implant after four weeks of healing period. The values of the elastic modulus and hardness were higher for the TiZr1317 implant than for the cpTi implant, although the difference was not significant [132]. A complementary study has shown that Young's modulus of newly formed bone tissue also depends on the implant surface treatment since the apparent indentation modulus (respectively the hardness) of periprosthetic bone was around 1.5 (respectively 3) times higher around acid-etched titanium than around machined titanium [6].

Atomic force microscopy (AFM) is another method used to study the mechanical properties of newly formed bone tissue near the BII and allows work at a lower scale than nanoindentation [64]. The principle of the measurements relies on the analysis of the deflection of a cantilever with a predetermined stiffness. The movement of the cantilever depends on the interactions between its tip and the studied surface and is monitored with a laser system. This set-up results in a force–displacement curve which leads to the elastic modulus and hardness of the material, similar to the case of nanoindentation [64,133].

In a study investigating osseointegration phenomena around titanium implants after four weeks of healing time, AFM was used to measure the surface profile. AFM was also used to measure the mechanical response of bone tissue based on the analysis of the curve representing the load as a function of the cantilever tip displacement. The measurements were carried out at different distances from implant surface in maxillary and femoral bone tissue. For implants inserted in maxillary bone tissue, the values of Young's modulus were between 1.04 ± 0.21 MPa and 1.21 ± 0.34 MPa and did not depend on the distance from the implant surface. In contrast, for implants inserted in femoral bone tissue, the values of Young's modulus were between 0.87 ± 0.25 MPa and 2.24 ± 0.69 MPa and were shown to significantly increase as a function of the distance from the implant surface (between 0–5 µm and 420 µm) [134]. However, the aforementioned values are very low compared with other Young's moduli (of the order of several GPa; table 3), and the reasons for such different orders of magnitude remain unclear.

One limitation of the AFM technique lies in that the geometry of the cantilever tip is not precisely known and errors are associated with the estimation of the displacements of the tip in all directions, leading to a lack of precision of the estimation of the elastic modulus and hardness of the investigated tissues. As a consequence, some AFM devices may also be used in a nanoindentation mode using a shape-defined diamond tip and an adapted load–displacement control [133]. Such a configuration was used to study bone tissues in bovine tibia and collagen fibrils in rat tail tendon, resulting in values of Young's moduli between 11.8 ± 3.6 and 14.1 ± 5.3 GPa [139] and between 5.0 and 11.5 GPa [140], respectively.

Furthermore, such a configuration was implemented to study the BII in an early study evidencing a lower indentation modulus of 6.17 GPa near the BII, which increases with a positive slope of 0.014 GPa μm^{-1} in the direction perpendicular to the implant surface until around 150 µm away from the interface. This last result suggests again the existence of a gradient of material properties at the BII, which could be explained by a strongly heterogeneous stress field near the BII, leading to different remodelling conditions [135].

In the aforementioned works, indents were often observed with an optical microscope to check that the indented regions of interest actually correspond to newly formed bone and not to resin or bone defect [6,135]. However, it was difficult to clearly distinguish between mature and newly formed bone tissue because both types of tissue were interconnected and difficult to clearly distinguish. In order to overcome the aforementioned limitation, we have implemented the implant model described in figure 5 in order to create a 200 µm thick bone chamber between mature bone and the implant surface [136–138]. The bone chamber was designed using PTFE layers, as shown in figure 5. No bone tissue was present in the bone chamber just after surgery and newly formed bone tissue grows in the bone chamber, which makes it possible to

Table 3. Summary of the microscopic biomechanical properties of newly formed tissues at the BII by indentation-based technique in the literature.

animal model			implant				biomechanical properties of newly formed tissue			
animal	newly formed tissue	healing period	material	surface treatment	surface roughness (R_a, µm)	testing configuration	distance from implants (µm)	Young's modulus (Pa)	hardness (GPa)	ref.
—	non-mineralized fibrous tissue	—		—	—	AFM	—	0–950.5 kPa	—	[64]
						nanoindentation		0–19 kPa		
Sprague–Dawley rats	mineralized bone tissue	2 weeks	titanium	machined surface	0.024 ± 0.005	nanoindentation	10–60	7.5 ± 1.07 G	0.18 ± 0.08	[6]
		4 weeks						8.33 ± 1.67 G	0.26 ± 0.03	
		2 weeks		acid-etching (HCl and H_2SO_4)	0.231 ± 0.051			12.50 ± 2.50 G	0.59 ± 0.15	
		4 weeks						12.50 ± 1.50 G	0.75 ± 0.13	
Sinclair miniswine	mineralized bone tissue	4 weeks	titanium	—	—	AFM nanoindentation	<150	7.78 ± 0.47 G	0.189 ± 0.015	[135]
							150–500	8.61 ± 0.45 G	0.209 ± 0.014	
							500–800	9.19 ± 0.48 G	0.215 ± 0.015	
							>800	9.01 ± 0.45 G	0.215 ± 0.014	
Göttingen mini pigs	mineralized mandibular bone tissue	4 weeks	commercially pure titanium (cpTi), titanium–zirconium alloy (TiZr1317)	sandblasted acid-etched hydrophilic surface	—	nanoindentation	cpTi	2.68 ± 0.51 G	0.110 ± 0.017	[132]
							TiZR1317	2.73 ± 0.50 G	0.116 ± 0.017	
New Zealand rabbits	mineralized cortical bone tissue	4 weeks	Ti6Al4V medical grade titanium alloy	TiO_2 blasting	1.9	nanoindentation	0–200	15.35 ± 1.81 G	0.643 ± 0.096	[136–138]
		7 weeks						15.85 ± 1.55 G	0.66 ± 0.101	
		13 weeks						17.82 ± 2.10 G	0.668 ± 0.074	

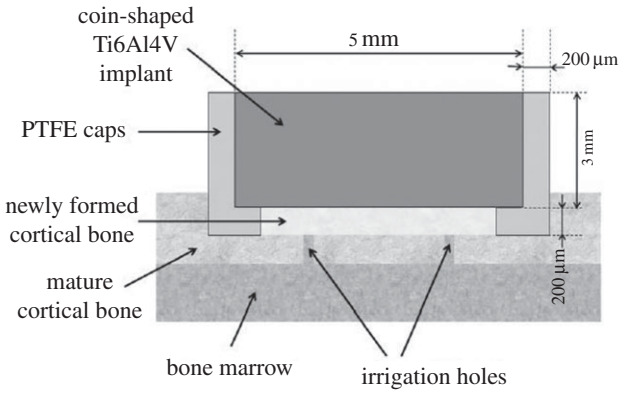

Figure 5. Schematic of the coin-shaped implant model including the bone chamber [136].

carry out nanoindentation measurements in newly formed bone only, and therefore to clearly distinguish mature and newly formed bone tissue. The results showed a significant increase in the apparent indentation modulus as a function of healing time, which may stem from an increase in bone mineralization [136–138].

The documented values of microscopic biomechanical properties of newly formed tissues around the BII are summarized in table 3. Non-mineralized fibrous tissue is shown to have a very low indentation modulus, close to that of soft tissue [64]. Cortical bone tissue seems stiffer than trabecular bone tissue [6,132,134–138].

However, whether nano-indentation or AFM plays any clinical role remains uncertain [141].

4.2. Quantitative ultrasound

Because ultrasound is a mechanical wave, quantitative ultrasound (QUS) techniques are naturally likely to retrieve bone mechanical properties. Another advantage of QUS techniques lies in that ultrasound is non-invasive (ultrasound is even used to stimulate osseointegration [142]), non-radiative and relatively cheap. Note that, in the context of osteoporosis assessment, QUS is now routinely used clinically to assess bone fragility [143].

It remains difficult to understand the physical phenomena occurring during the interaction between an ultrasonic wave and the BII, owing to the complex nature of the BII. Therefore, different finite-element models have been implemented because modelling and simulation allow the influence of all bone properties (such as compression and shear modulus and mass density) on the ultrasonic response of the BII to be distinguished in a controlled configuration, which is not easy to achieve experimentally because all bone properties vary in parallel. Ultrasound propagation in a dental implant has been modelled using finite-element modelling, allowing the dependence of its echographic response on the properties of periprosthetic bone tissue to be derived [144,145]. A limitation of the aforementioned approach lies in that the BII was assumed to be fully bounded and that the roughness was not considered. More recently, a finite-element model [146] was developed accounting for the implant roughness as well as for a soft tissue layer corresponding to fibrous tissue. This study showed that the reflection coefficient of an ultrasound wave on the BII depends on the properties of bone tissue located at a distance of between 1 and 25 µm from the implant surface, thus opening a new path in the investigation of the BII properties. The three aforementioned modelling studies [144–146] showed that QUS techniques around 10 MHz are sensitive to changes of bone properties occurring at a distance lower than around 15 µm from the implant surface.

Experimental models may also be employed to retrieve information on the QUS response of the BII. The echographic response of BII [20] was studied using the coin-shaped implant model described in figure 5, which is advantageous because of the planar BII, which allows experimentation under standardized conditions. The amplitude of the echo of the BII measured at around 15 MHz was shown to decrease as a function of healing time. This result can be explained by the increase of bone quality and quantity around the implant surface, which leads to a decrease in the gap of the mechanical properties at the BII during healing.

The same coin-shaped implant model has also been used in combination with micro-Brillouin scattering, a technique consisting of exploiting the coupling of laser and ultrasound in order to retrieve the ultrasonic velocity at the same scale (several micrometres) as the nanoindentation measurements described in the last subsection [19,137]. The results showed that the ultrasonic velocity at the microscale in newly formed bone tissue and in mature bone tissue was significantly different and equal to around 4930 and 5250 m s^{-1}, respectively [137]. Coupling nanoindentation and micro-Brillouin scattering allowed two complementary bone properties to be retrieved (the apparent indentation modulus and the ultrasonic velocity) at the same scale. Comparing the indentation modulus and the ultrasonic velocity showed that the mass density of mature bone tissue is around 13% higher than mass density of newly formed bone tissue at the scale of several micrometres [137]. This last result can be explained by the increase in mineralization during bone tissue ageing.

4.3. Other promising approaches

Many authors have investigated the properties of bone tissue in the bulk, but relatively few have focused on periprosthetic tissue, in particular because of the difficulty of simultaneously obtaining an adapted sample and carrying out complex multimodality experiments. The investigation of the BII at the nano-scale is of particular interest when studying implant anchorage, as bone rupture starts between collagen fibres and the hydroxyapatite crystals [147]. Different techniques, such as X-ray, neutron and electron-based techniques, and spectroscopy, have been employed and are described below.

4.3.1. X-ray-based techniques

Optical microscopy techniques are often used to observe biological tissues, but they consist in analysing two-dimensional sections. To improve such analysis, three-dimensional techniques have been developed such as X-ray µCT [148,149], which allows imaging of woven bone formation at a titanium interface at the microscale [150] for further finite-element analysis at the microscopic level [151].

X-ray diffraction techniques [152–157] and *small-angle x-ray scattering* (SAXS) [158] have been used to characterize the inorganic structure of bulk bone, such as the shape and orientation of hydroxyapatite crystals. Little work has been done using SAXS to investigate the periprosthetic bone tissue. The mineral crystals close to the implant surface were found to be preferentially aligned with the implant surface [158]. However, no work has been done on the evolution of this alignment over time and space during osseointegration.

X-ray diffraction investigates intensity ratios, which indicate the *c*-axis orientation of biological apatite (BAp) in bone [153,155–157]. Such a technique shows that the BAp crystal *c*-axis orientation is often parallel to the existing collagen fibres [153]. Note that the orientation of newly formed collagen fibres is approximately parallel to the existing collagen fibres [156]. Furthermore, the BAp crystal preferential alignment follows the local stress distribution, as has been shown in the mandible near the tooth because of mastication forces [153,155]. Therefore, orientation quantities (intensity ratio of the peak characteristics of the BAp *c*-axis, tilt angle) appear to be related to diverse bone properties such as the ultrasonic wave velocity [154], Young's modulus [156] and microhardness [159]. The BAp crystal orientation is thus an interesting indicator for mechanical bone properties. Likewise, X-ray diffractometers have been used to study the alignment of BAp crystals in comparison with the stress distribution and the orientation of grooves on the surface of a hip implant [160] or at the neck of dental implants [161].

Roentgen stereophotogrammetry analysis (RSA), also called radiostereometry, is a radiographic observation technique aimed at obtaining a three-dimensional motion analysis, initiated by Selvik in 1989 [162]. Comparing with ordinary radiography, RSA shows a much higher resolution owing to the metallic markers, such as small tantalum balls, injected in the bone and on the implant surface that allow analysis of very small movement [163,164], thus providing a promising non-invasive measurement to assess joint replacement, such as prosthetic fixation, joint kinematics as well as stability of implant [39,40,165].

4.3.2. Neutron-based techniques

Neutron microcomputed tomography is a promising technique to investigate the BII because of the absence of metal artefacts obtained with X-ray-based techniques. A dental implant integrated in a rat tibia has been investigated with both X-rays and neutron tomography at different resolutions [166]. Bone in-growth was shown to be equivalent for all images except with the neutron images of the lowest resolution. Neutron tomography was then used in combination with the pull-out test [167]. As a result, neutron images allowed bone growth to be quantified at the interface without artefacts and the images were analysed to follow the evolution of strains and cracks in the surrounding bone as the implant was pulled-out and until BII failure.

4.3.3. Electron-based techniques

Electron tomography is another promising technique allowing visualization of the three-dimensional structure at a high resolution [168]. Electron tomography was used to investigate in three dimensions the interface between human bone and a hydroxyapatite implant, which allowed the observation, at the nanometre scale, of hydroxyapatite crystal orientation around the implant surface in comparison with the orientation of crystals in the collagen matrix of bone. Another function of electron tomography is elemental analysis [148], as in [169], which provides elemental mapping of Ca, P, O and Ti at the implant interface. Electron tomography samples can be prepared with the focused ion beam (FIB) method, thus producing thin lamella [148,150].

4.3.4. Spectroscopic approaches

Two spectroscopic methods (Fourier-transform infrared spectroscopy (FTIR) and Raman spectroscopy) have been employed to characterize the composition of mature and newly formed bone tissue. These two techniques have been used to study the structural changes in bone tissue depending on the distance to the implant during osseointegration around an artificial composite bone material [170]. FTIR spectroscopy allows characterization of bone mineral and matrix components by comparing the results with a reference spectrum. The components provide information on bone microstructural properties such as mineral content, crystallinity and collagen maturity at the nanometre scale owing to the combination of FTIR and AFM techniques [171].

On the other hand, Raman spectroscopy provides similar information to FTIR spectroscopy on samples of various types and with easier sample preparation. The drawbacks of Raman spectroscopy compared with FTIR are a lower signal-to-noise ratio and possible fluorescence. In a study carried out in bone tissue, the parameters derived from the analysis of the Raman spectra have been shown to be related to the bone biomechanical properties, and their correlation depends on the animal's age [172,173]. Raman spectroscopy has also been used to study the BII in an *in vivo* study with three-dimensional printed Ti6Al4V implants after six-month healing in sheep femora. The Raman analysis was used to characterize the molecular composition of both native and newly formed bone tissue at the BII [174].

5. Influence of the implant properties

During bone healing, the evolution of the properties of newly formed bone tissue described in the previous section depends on many factors, including implant stiffness and implant surface topology, which will be discussed below.

5.1. Implant stiffness

The majority of endosseous implants are made of commercially pure titanium or titanium alloy for oral implants and of titanium alloys, chrome-cobalt molybdenum alloys and stainless steel for orthopaedic implants because of their excellent biocompatibility, corrosion resistance and high strength-to-weight ratio [175]. However, a common problem, referred to as stress shielding in the literature, is related to the contrast of density and stiffness between bone and the implant, which may cause inhomogeneous stress distribution and stress concentration at the vicinity of the implant, thus increasing the risks of implant failure. Stress-shielding effects have been shown to be important for orthopaedic implants but are less significant around dental implants [176,177].

A stiffer orthopaedic implant is known to lead to a higher level of bone mineral loss in the vicinity of the implant [178]. Similar results have been obtained using finite-element studies [179,180]. Thomas & Cook [113] systematically investigated the effect of the elastic modulus of an implant on shear stiffness and strength of the BII. The elastic modulus of the implant material covered a large range of variation, from 3 GPa (polymethyl methacrylate, PMMA) to 385 GPa (Al_2O_3). The authors reported no significant effect of the implant stiffness on the mechanical properties of the BII. However, a large range of variation in the results on interface strength and stiffness in each tested group was obtained, which might come from inter-individual variations as well as from variations in the surface roughness that was not controlled. Gottlow *et al.* [181] demonstrated that implants made of titanium–zirconium alloy (TiZr1317) with lower stiffness and similar surface

treatment and implant geometries presented higher removal torque than cpTi implants. In order to decrease the effects due to stress shielding, another approach consists in developing customized porous implants using three-dimensional printing technology [182] or laser power-bed fusion [91]. Other studies attempted to develop Ti-based metallic materials with lower stiffness, improving bone remodelling to enhance mechanical properties of the BII [183–185]. However, the variation in surface composition between implants may also influence the results, which makes it difficult to attribute the difference in terms of osseointegration to stress-shielding effects only.

5.2. Implant surface

Biomaterial surfaces may undergo various modifications affecting their physical, chemical and viscoelastic properties [186] in order to obtain an optimal surface topography, which has been shown to influence osseointegration [5,187]. Surface roughness not only enhances primary stability, as mentioned in §3.2, but also stimulates bone tissue repair [6,188]. However, a compromise should be found concerning the roughness level of the implant surface. Wennerberg & Albrektsson [141] were the first authors to clearly differentiate between smooth, minimally rough, moderately rough and rough surfaces and to describe a peak in the bone response for moderately rough surfaces. As reviewed in [141], moderately rough (S_a between 1 and 2 µm) surfaces showed stronger bone responses than smooth ($S_a <$ 0.5 µm), minimally rough (S_a between 0.5 and 1 µm) and rough ($S_a > 2$ µm) implant surfaces. In another study, the optimal value of S_a (defined by the average height deviation from the surface) optimizing osseointegration was shown to be around 3.6–3.9 µm [22,118]. However, the experiments described in [22,118] were realized with a simple coin-shaped implant model generating a low level of mechanical stresses within bone tissue because of the implant's specific macroscopic geometrical configuration without any threading. The roughness should be sufficiently high in order to stimulate bone remodelling but not too high because excessive roughness may create stress concentration and debris, damaging bone tissue and thus hampering osseointegration processes.

As indicated in tables 1–3, most surface topographical analyses were done using the so-called R_a values and were evaluated with stylus instruments, which constitutes a strong limitation because such an approach does not provide reliable evaluations of the true surface roughness [141]. Wennerberg & Albrektsson [189] systematically evaluated three main types of measurement—mechanical contact profilometers, optical profiling instruments, scanning probe microscopes—with their advantages and disadvantages in implant research. Optical profiling instruments, such as interferometry, were suggested to be the most suitable method for assessing surface roughness since they can process measurements of complex geometries and be effective at the micrometre level of resolution, which is the clinically relevant one. Anything but three-dimensional S_a analyses seems of limited interest. Surface roughness analysis must be investigated in relevant areas of the bone-anchored parts of implants and not in irrelevant flat surfaces never in contact with bone tissue [189]. Many studies [22,108–111,114,117–121] documented a height deviation parameter, R_a/S_a, that describes surface roughness, as shown in table 2; also, as reviewed in [141], a combination of R_a/S_a, spatial and hybrid parameters (such as *Sdr%* defined in [141]) would be a standard to provide a better surface characterization for modern implants.

6. Conclusion

Understanding the biomechanical behaviour of the BII is a difficult problem because bone is a complex medium, which evolves in time due to remodelling phenomena. The presence of a rough interface complicates the situation by creating complex multi-axial stress around the implant surface. The difficulty also comes from the multi-factorial determinants of the problem, given by the implant properties (determined by the implant manufacturer), by the surgical protocol (which is not standardized) and by the patient's bone quality and behaviour. The phenomena responsible for implant osseointegration are far from being understood, and measuring periprosthetic bone properties remains a challenge.

The ultimate dream of patients and surgeons would be to be able to understand and eventually to predict implant evolution as a function of the environment, in order to provide a decision support system that could be designed using, for example, deep learning-based approaches in a patient-specific manner. To reach this long-term goal, a better understanding of the biomechanical phenomena is needed, which can be achieved through the coupling of experimental surgery with multi-modality measurement approaches providing complementary information on the evolution of periprosthetic bone tissue. In particular, acoustic methods are promising because they may be used to provide information on the bone biomechanical properties non-invasively. However, experimental techniques remain limited to understanding the basic phenomena because it is impossible to control all bone properties, which vary in parallel. Therefore, dedicated mechanical models must be developed in parallel with the experiments. These models should in particular account for the adhesive contact at the BII as well as for the roughness of the implant, in both the static and dynamic regimes.

A better understanding of the basic phenomena will lead to (i) the development of medical devices that help surgeons to determine an implant's stability both during and after surgery and (ii) useful information for the implant manufacturer to improve the quality of their product.

Data accessibility. This article has no additional data.

Competing interests. We declare we have no competing interests.

Funding. This project has received funding from the European Research Council (ERC) under the European Union's Horizon 2020 research and innovation program (grant agreement no. 682001, project ERC Consolidator Grant 2015 BoneImplant).

References

1. Williams DL, Isaacson BM. 2014 The 5 hallmarks of biomaterials success: an emphasis on orthopaedics. *Adv. Biosci. Biotechnol.* **2014**, 283–293.

2. Gao X, Sevostianov I. 2016 Connection between elastic and electrical properties of cortical bone.

J. Biomech. **49**, 765–772. (doi:10.1016/j.jbiomech.2016.02.019)

3. Wolff J. 1986 *The law of bone remodeling*. Berlin, Germany: Springer.
4. Winter W, Heckmann SM, Weber HP. 2004 A time-dependent healing function for immediate loaded implants. *J. Biomech.* **37**, 1861–1867. (doi:10.1016/j.jbiomech.2004.02.033)
5. Schwartz Z, Nasazky E, Boyan BD. 2005 Surface microtopography regulates osteointegration: the role of implant surface microtopography in osteointegration. *Alpha Omegan* **98**, 9–19.
6. Butz F, Aita H, Wang CJ, Ogawa T. 2006 Harder and stiffer bone osseointegrated to roughened titanium. *J. Dent. Res.* **85**, 560–565. (doi:10.1177/154405910608500616)
7. Hansson S. 2000 Surface roughness parameters as predictors of anchorage strength in bone: a critical analysis. *J. Biomech.* **33**, 1297–1303. (doi:10.1016/S0021-9290(00)00045-2)
8. Brunski JB. 1999 *In vivo* bone response to biomechanical loading at the bone/dental-implant interface. *Adv. Dent. Res.* **13**, 99–119. (doi:10.1177/08959374990130012301)
9. Dodd CA, Hungerford DS, Krackow KA. 1990 Total knee arthroplasty fixation. Comparison of the early results of paired cemented versus uncemented porous coated anatomic knee prostheses. *Clin. Orthop. Relat. Res.* **260**, 66–70. (doi:10.1097/00003086-199011000-00013)
10. Donaldson AJ, Thomson HE, Harper NJ, Kenny NW. 2009 Bone cement implantation syndrome. *Br. J. Anaesth.* **102**, 12–22. (doi:10.1093/bja/aen328)
11. Puleo DA, Nanci A. 1999 Understanding and controlling the bone-implant interface. *Biomaterials* **20**, 2311–2321. (doi:10.1016/S0142-9612(99)00160-X)
12. Junker R, Dimakis A, Thoneick M, Jansen JA. 2009 Effects of implant surface coatings and composition on bone integration: a systematic review. *Clin. Oral Implants Res.* **20**(Suppl 4), 185–206. (doi:10.1111/j.1600-0501.2009.01777.x)
13. Skoric J, Seiler C. 2014 Osseointegration: a review of the fundamentals for assuring cementless skeletal fixation. *Orthop. Res. Rev.* **2014**, 370–377.
14. Liu X, Chu PK, Ding C. 2004 Surface modification of titanium, titanium alloys, and related materials for biomedical applications. *Mater. Sci. Eng. R Rep.* **47**, 49–121. (doi:10.1016/j.mser.2004.11.001)
15. Lenneras M, Palmquist A, Norlindh B, Emanuelsson L, Thomsen P, Omar O. 2015 Oxidized titanium implants enhance osseointegration via mechanisms involving RANK/RANKL/OPG regulation. *Clin. Implant Dent. Relat. Res.* **17**(Suppl 2), e486–e500. (doi:10.1111/cid.12276)
16. Omar O, Svensson S, Suska F, Emanuelsson L, Hall J, Nannmark U, Thomsen P. 2010 Integrin and chemokine receptor gene expression in implant-adherent cells during early osseointegration. *J. Mater. Sci. Mater. Med.* **21**, 969–980. (doi:10.1007/s10856-009-3915-x)
17. Omar OM, Suska F, Emanuelsson L, Hall JM, Palmquist A, Thomsen P. 2011 The correlation between gene expression of proinflammatory markers and bone formation during osseointegration with titanium implants. *Biomaterials* **32**, 374–386. (doi:10.1016/j.biomaterials.2010.09.011)
18. Palmquist, A *et al*. 2010 Titanium oral implants: surface characteristics, interface biology and clinical outcome. *J. R. Soc. Interface* **7**(Suppl 5), S515–S527. (doi:10.1098/rsif.2010.0118.focus)
19. Mathieu V, Vayron R, Richard G, Lambert G, Naili S, Meningaud J-P, Haiat G. 2014 Biomechanical determinants of the stability of dental implants: influence of the bone-implant interface properties. *J. Biomech.* **47**, 3–13. (doi:10.1016/j.jbiomech.2013.09.021)
20. Mathieu V, Vayron R, Soffer E, Anagnostou F. 2012 Influence of healing time on the ultrasonic response of the bone-implant interface. *Ultrasound Med. Biol.* **38**, 611–618. (doi:10.1016/j.ultrasmedbio.2011.12.014)
21. Bolind P *et al*. 2005 A study of 275 retrieved Branemark oral implants. *Int. J. Periodontics Restorative Dent.* **25**, 425–437.
22. Ronold HJ, Ellingsen JE. 2002 Effect of micro-roughness produced by TiO_2 blasting–tensile testing of bone attachment by using coin-shaped implants. *Biomaterials* **23**, 4211–4219. (doi:10.1016/S0142-9612(02)00167-9)
23. Johansson C, Albrektsson T. 1987 Integration of screw implants in the rabbit: a 1-yr follow-up of removal torque of titanium implants. *Int. J. Oral Maxillofac. Implants* **2**, 69–75.
24. Branemark P-I. 1977 Osseointegrated implants in the treatment of the edentulous jaw. Experience from a 10-year period. *Scand. J. Plast. Reconstr. Surg.* **16**, 1–132.
25. Liu S, Broucek J, Virdi AS, Sumner DR. 2012 Limitations of using micro-computed tomography to predict bone-implant contact and mechanical fixation. *J. Microsc.* **245**, 34–42. (doi:10.1111/j.1365-2818.2011.03541.x)
26. Potter HG, Nestor BJ, Sofka CM, Ho ST, Peters LE, Salvati EA. 2004 Magnetic resonance imaging after total hip arthroplasty: evaluation of periprosthetic soft tissue. *J. Bone Joint Surg. Am.* **86-A**, 1947–1954. (doi:10.2106/00004623-200409000-00013)
27. Berahmani S, Janssen D, van Kessel S, Wolfson D, de Waal Malefijt M, Buma P, Verdonschot N. 2015 An experimental study to investigate biomechanical aspects of the initial stability of press-fit implants. *J. Mech. Behav. Biomed. Mater.* **42**, 177–185. (doi:10.1016/j.jmbbm.2014.11.014)
28. Shirazi-Adl A, Forcione A. 1992 Finite element stress analysis of a push-out test. Part II: Free interface with nonlinear friction properties. *J. Biomech. Eng.* **114**, 155–161. (doi:10.1115/1.2891366)
29. Shultz TR, Blaha JD, Gruen TA, Norman TL. 2006 Cortical bone viscoelasticity and fixation strength of press-fit femoral stems: finite element model. *J. Biomech. Eng.* **128**, 7–12. (doi:10.1115/1.2133765)
30. Shirazi-Adl A, Dammak M, Paiement G. 1993 Experimental determination of friction characteristics at the trabecular bone/porous-coated metal interface in cementless implants. *J. Biomed. Mater. Res.* **27**, 167–175. (doi:10.1002/jbm.820270205)
31. Chong DY, Hansen UN, Amis AA. 2010 Analysis of bone-prosthesis interface micromotion for cementless tibial prosthesis fixation and the influence of loading conditions. *J. Biomech.* **43**, 1074–1080. (doi:10.1016/j.jbiomech.2009.12.006)
32. ten Broeke RH, Tarala M, Arts JJ, Janssen DW, Verdonschot N, Geesink RGT. 2014 Improving peri-prosthetic bone adaptation around cementless hip stems: a clinical and finite element study. *Med. Eng. Phys.* **36**, 345–353. (doi:10.1016/j.medengphy.2013.12.006)
33. Gortchacow M, Wettstein M, Pioletti DP, Terrier A. 2011 A new technique to measure micromotion distribution around a cementless femoral stem. *J. Biomech.* **44**, 557–560. (doi:10.1016/j.jbiomech.2010.09.023)
34. Suarez DR, Valstar ER, Rozing PM, van Keulen F. 2013 Fracture risk and initial fixation of a cementless glenoid implant: the effect of numbers and types of screws. *Proc. Inst. Mech. Eng. H* **227**, 1058–1066. (doi:10.1177/0954411913491050)
35. Gaines Jr RW. 2000 The use of pedicle-screw internal fixation for the operative treatment of spinal disorders. *J. Bone Joint Surg. Am.* **82–A**, 1458–1476. (doi:10.2106/00004623-200010000-00013)
36. Cuny C, Scarlat MM, Irrazi M, Beau P, Wenger V, Ionescu N, Berrichi A. 2008 The Telegraph nail for proximal humeral fractures: a prospective four-year study. *J. Shoulder Elbow Surg.* **17**, 539–545. (doi:10.1016/j.jse.2008.02.004)
37. Duyck J, Vandamme K, Geris L, Van Oosterwyck H, De Cooman M, Vandersloten J, Puers R, Naert I. 2006 The influence of micro-motion on the tissue differentiation around immediately loaded cylindrical turned titanium implants. *Arch. Oral Biol.* **51**, 1–9. (doi:10.1016/j.archoralbio.2005.04.003)
38. Taylor M, Barrett DS, Deffenbaugh D. 2012 Influence of loading and activity on the primary stability of cementless tibial trays. *J. Orthop. Res.* **30**, 1362–1368. (doi:10.1002/jor.22056)
39. Fukuoka S, Yoshida K, Yamano Y. 2000 Estimation of the migration of tibial components in total knee arthroplasty. A roentgen stereophotogrammetric analysis. *J. Bone Joint Surg. Br.* **82**, 222–227. (doi:10.1302/0301-620X.82B2 .9461)
40. Ryd L, Albrektsson BE, Carlsson L, Dansgard F, Herberts P, Lindstrand A, Regner L, Toksvig-Larsen S. 1995 Roentgen stereophotogrammetric analysis as a predictor of mechanical loosening of knee prostheses. *J. Bone Joint Surg. Br.* **77**, 377–383. (doi:10.1302/0301-620X.77B3.7744919)
41. Duyck J *et al*. 2010 Histological, histomorphometrical, and radiological evaluation of an experimental implant design with a high insertion torque. *Clin. Oral Implants Res.* **21**, 877–884. (doi:10.1111/j.1600-0501.2010.01895.x)

42. Coelho PG, Granato R, Marin C, Bonfante EA, Freire JNO, Janal MN, Gil JN, Suzuki M. 2010 Biomechanical evaluation of endosseous implants at early implantation times: a study in dogs. *J. Oral Maxillofac. Surg.* **68**, 1667–1675. (doi:10.1016/j.joms.2010.02.050)
43. Cowin S. 1986 Wolff's law of trabecular architecture at remodeling equilibrium. *J. Biomech. Eng.* **108**, 83–88. (doi:10.1115/1.3138584)
44. Swan CC, Lakes RS, Brand RA, Stewart KJ. 2003 Micromechanically based poroelastic modeling of fluid flow in Haversian bone. *J. Biomech. Eng.* **125**, 25–37. (doi:10.1115/1.1535191)
45. Checa S, Prendergast PJ. 2009 A mechanobiological model for tissue differentiation that includes angiogenesis: a lattice-based modeling approach. *Ann. Biomed. Eng.* **37**, 129–145. (doi:10.1007/s10439-008-9594-9)
46. Davies PF. 2009 Hemodynamic shear stress and the endothelium in cardiovascular pathophysiology. *Nat. Clin. Pract. Cardiovasc. Med.* **6**, 16–26. (doi:10.1038/ncpcardio1397)
47. Sansalone V, Kaiser J, Naili S, Lemaire T. 2013 Interstitial fluid flow within bone canaliculi and electro-chemo-mechanical features of the canalicular milieu: a multi-parametric sensitivity analysis. *Biomech. Model. Mechanobiol.* **12**, 533–553. (doi:10.1007/s10237-012-0422-7)
48. Lemaire T, Kaiser J, Naili S, Sansalone V. 2012 Parametric study of interstitial fluid flow in the bone lacuno-canalicular network. *Comput. Methods Biomech. Biomed. Engin.* **15**(Suppl 1), 331–332. (doi:10.1080/10255842.2012.713683)
49. Lai X, Price C, Modla S, Thompson WR, Caplan J, Kirn-Safran CB, Wang L. 2015 The dependences of osteocyte network on bone compartment, age, and disease. *Bone Res.* **3**, 15009. (doi:10.1038/boneres.2015.9)
50. Langer M, Pacureanu A, Suhonen H, Grimal Q, Cloetens P, Peyrin F. 2012 X-ray phase nanotomography resolves the 3D human bone ultrastructure. *PLoS ONE* **7**, e35691. (doi:10.1371/journal.pone.0035691)
51. Marotti G, Ferretti M, Remaggi F, Palumbo C. 1995 Quantitative evaluation on osteocyte canalicular density in human secondary osteons. *Bone* **16**, 125–128. (doi:10.1016/8756-3282(95)80022-I)
52. Lemaire T, Naili S, Remond A. 2008 Study of the influence of fibrous pericellular matrix in the cortical interstitial fluid movement with hydroelectrochemical effects. *J. Biomech. Eng.* **130**, 011001. (doi:10.1115/1.2838025)
53. Mori S, Makino T, Koyama D, Takayanagi S, Yanagitani T, Matsukawa M. 2018 Ultrasonically-induced electrical potentials in demineralized bovine cortical bone. *AIP Adv.* **8**, 045007. (doi:10.1063/1.5022138)
54. Matsukawa M, Matsukawa S. 2017 Study on ultrasound irradiation induction of electrical potentials in bone. *J. Orthop. Trauma* **31**, S4. (doi:10.1097/01.bot.0000520896.84846.64)
55. Lemaire T, Pham TT, Capiez-Lernout E, de Leeuw NH, Naili S. 2015 Water in hydroxyapatite nanopores: possible implications for interstitial bone fluid flow. *J. Biomech.* **48**, 3066–3071. (doi:10.1016/j.jbiomech.2015.07.025)
56. Martin M, Lemaire T, Pivonka P, Sansalone V. 2017 A thermodynamically consistent model of bone rotary remodeling: a 2D study. *Comput. Methods Biomech. Biomed. Engin.* **20**(Suppl 1), 127–128. (doi:10.1080/10255842.2017.1382894)
57. Geesink RG, de Groot K, Klein CP. 1987 Chemical implant fixation using hydroxyl-apatite coatings: the development of a human total hip prosthesis for chemical fixation to bone using hydroxyl-apatite coatings on titanium substrates. *Clin. Orthop. Relat. Res.* **225**, 147–170. (doi:10.1097/00003086-198712000-00014)
58. Biemond JE, Verdonschot N, Buma P. 2011 Frictional and bone ingrowth properties of engineered surface topographies produced by electron beam technology. *Arch. Orthop. Trauma Surg.* **131**, 711–718. (doi:10.1007/s00402-010-1218-9)
59. Shah FA, Thomsen P, Palmquist A. 2019 Osseointegration and current interpretations of the bone-implant interface. *Acta Biomater.* **84**, 1–15. (doi:10.1016/j.actbio.2018.11.018)
60. Mori S, Burr DB. 1993 Increased intracortical remodeling following fatigue damage. *Bone* **14**, 103–109. (doi:10.1016/8756-3282(93)90235-3)
61. Bragdon CR, Burke D, Lowenstein JD, O'Connor DO, Ramamurti B, Jasty M, Harris WH. 1996 Differences in stiffness of the interface between a cementless porous implant and cancellous bone *in vivo* in dogs due to varying amounts of implant motion. *J. Arthroplasty* **11**, 945–951. (doi:10.1016/S0883-5403(96)80136-7)
62. Pilliar RM, Lee JM, Maniatopoulos C. 1986 Observations on the effect of movement on bone ingrowth into porous-surfaced implants. *Clin. Orthop. Relat. Res.* **208**, 108–113. (doi:10.1097/00003086-198607000-00023)
63. Engh CA *et al.* 1992 Quantification of implant micromotion, strain shielding, and bone resorption with porous-coated anatomic medullary locking femoral prostheses. *Clin. Orthop. Relat. Res.* **285**, 13–29. (doi:10.1097/00003086-199212000-00005)
64. Moerman A, Zadpoor AA, Oostlander A, Schoeman M, Rahnamay MP, Pouran B, Valstar E. 2016 Structural and mechanical characterisation of the peri-prosthetic tissue surrounding loosened hip prostheses. An explorative study. *J. Mech. Behav. Biomed. Mater.* **62**, 456–467. (doi:10.1016/j.jmbbm.2016.04.009)
65. Haynes DR, Rogers SD, Hay S, Pearcy MJ, Howie DW. 1993 The differences in toxicity and release of bone-resorbing mediators induced by titanium and cobalt-chromium-alloy wear particles. *J. Bone Joint Surg. Am.* **75**, 825–834. (doi:10.2106/00004623-199306000-00004)
66. Moreschini O, Fiorito S, Magrini L, Margheritini F, Romanini L. 1997 Markers of connective tissue activation in aseptic hip prosthetic loosening. *J. Arthroplasty* **12**, 695–703. (doi:10.1016/S0883-5403(97)90144-3)
67. Meredith N, Alleyne D, Cawley P. 1996 Quantitative determination of the stability of the implant-tissue interface using resonance frequency analysis. *Clin. Oral Implants Res.* **7**, 261–267. (doi:10.1034/j.1600-0501.1996.070308.x)
68. Friberg B, Sennerby L, Linden B, Lekholm U. 1999 Stability measurements of one-stage Brånemark implants during healing in mandibles: a clinical resonance frequency analysis study. *Int. J. Oral Maxillofac. Surg.* **28**, 266–272. (doi:10.1016/S0901-5027(99)80156-8)
69. Barewal RM *et al*. 2003 Resonance frequency measurement of implant stability *in vivo* on implants with a sandblasted and acid-etched surface. *Int. J. Oral Maxillofac. Implants* **18**, 641–651.
70. Valderrama P, Oates TW, Jones AA, Simpson J, Schoolfield JD, Cochran DL. 2007 Evaluation of two different resonance frequency devices to detect implant stability: a clinical trial. *J. Periodontol.* **78**, 262–272. (doi:10.1902/jop.2007.060143)
71. Lages FS, Douglas-de Oliveira DW, Costa FO. 2018 Relationship between implant stability measurements obtained by insertion torque and resonance frequency analysis: a systematic review. *Clin. Implant Dent. Relat. Res.* **20**, 26–33. (doi:10.1111/cid.12565)
72. Zanetti EM *et al.* 2018 Clinical assessment of dental implant stability during follow-up: what is actually measured, and perspectives. *Biosensors* (*Basel*) **8**, 68. (doi:10.3390/bios8030068)
73. Harrison N, McHugh PE, Curtin W, Mc Donnell P. 2013 Micromotion and friction evaluation of a novel surface architecture for improved primary fixation of cementless orthopaedic implants. *J. Mech. Behav. Biomed. Mater.* **21**, 37–46. (doi:10.1016/j.jmbbm.2013.01.017)
74. Abdul-Kadir MR, Hansen U, Klabunde R, Lucas D, Amis A. 2008 Finite element modelling of primary hip stem stability: the effect of interference fit. *J. Biomech.* **41**, 587–594. (doi:10.1016/j.jbiomech.2007.10.009)
75. Bergmann G, Deuretzbacher G, Heller M, Graichen F, Rohlmann A, Strauss J, Duda GN. 2001 Hip contact forces and gait patterns from routine activities. *J. Biomech.* **34**, 859–871. (doi:10.1016/S0021-9290(01)00040-9)
76. Ledet EH, Westerhoff P, Szivek JA, Wachs RA, Bergmann G. 2012 Implantable sensor technology: from research to clinical practice. *J. Am. Acad. Orthop. Surg.* **20**, 383–392. (doi:10.5435/JAAOS-20-06-383)
77. Kutzner I, Heinlein B, Graichen F, Bender A, Rohlmann A, Halder A, Beier A, Bergmann G. 2010 Loading of the knee joint during activities of daily living measured *in vivo* in five subjects. *J. Biomech.* **43**, 2164–2173. (doi:10.1016/j.jbiomech.2010.03.046)
78. Nikooyan AA, Veeger HEJ, Westerhoff P, Graichen F, Bergmann G, van der Helm FCT. 2010 Validation of the Delft Shoulder and Elbow Model using *in-vivo* glenohumeral joint contact forces. *J. Biomech.* **43**, 3007–3014. (doi:10.1016/j.jbiomech.2010.06.015)
79. Bishop NE, Burton A, Maheson M, Morlock MM. 2010 Biomechanics of short hip endoprostheses—the risk of bone failure increases with decreasing

implant size. *Clin. Biomech. (Bristol, Avon)* **25**, 666–674. (doi:10.1016/j.clinbiomech.2010.04.013)

80. Nadorf J, Kinkel S, Gantz S, Jakubowitz E, Kretzer JP. 2017 Tibial revision knee arthroplasty with metaphyseal sleeves: the effect of stems on implant fixation and bone flexibility. *PLoS ONE* **12**, e0177285. (doi:10.1371/journal.pone.0177285)
81. Tijou A, Rosi G, Albini Lomami H, Hernigou P, Flouzat-Lachaniette CH, Haíat G. 2018 Monitoring cementless femoral stem insertion by impact analyses: an *in vitro* study. *J. Mech. Behav. Biomed. Mater.* **88**, 102–108. (doi:10.1016/j.jmbbm.2018.08.009)
82. Bolind P *et al*. 2005 A study of 275 retrieved Brånemark oral implants. *Int. J. Periodontics Restorative Dent.* **25**, 425–437.
83. Enoksen CH, Wik TS, Klaksvik J, Arthursson AJ, Husby OS, Gjerdet NR. 2017 Load transfer in the proximal femur and primary stability of a cemented and uncemented femoral stem: an experimental study on cadaver femurs. *Proc. Inst. Mech. Eng. H* **231**, 1195–1203. (doi:10.1177/0954411917737804)
84. Baleani M, Cristofolini L, Toni A. 2000 Initial stability of a new hybrid fixation hip stem: experimental measurement of implant-bone micromotion under torsional load in comparison with cemented and cementless stems. *J. Biomed. Mater. Res.* **50**, 605–615. (doi:10.1002/(SICI)1097-4636(20000615)50:4<605::AID-JBM17>3.0.CO;2-P)
85. Cristofolini L, Varini E, Viceconti M. 2007 *In-vitro* method for assessing femoral implant-bone micromotions in resurfacing hip implants under different loading conditions. *Proc. Inst. Mech. Eng. H* **221**, 943–950. (doi:10.1243/09544119JEIM278)
86. Bieger R, Ignatius A, Decking R, Claes L, Reichel H. 2012 Primary stability and strain distribution of cementless hip stems as a function of implant design. *Clin. Biomech. (Bristol, Avon)* **27**, 158–164. (doi:10.1016/j.clinbiomech.2011.08.004)
87. Bieger R, Ignatius A, Reichel H. 2013 Biomechanics of a short stem: *in vitro* primary stability and stress shielding of a conservative cementless hip stem. *J. Orthop. Res.* **31**, 1180–1186. (doi:10.1002/jor.22349)
88. Fehring KA, Owen JR, Kurdin AA, Wayne JS, Jiranek WA. 2014 Initial stability of press-fit acetabular components under rotational forces. *J. Arthroplasty* **29**, 1038–1042. (doi:10.1016/j.arth.2013.10.009)
89. Amirouche F, Solitro G, Broviak S, Goldstein W, Gonzalez M, Barmada R. 2015 Primary cup stability in THA with augmentation of acetabular defect. A comparison of healthy and osteoporotic bone. *Orthop. Traumatol. Surg. Res.* **101**, 667–673. (doi:10.1016/j.otsr.2015.07.007)
90. Amirouche F, Solitro G, Broviak S, Gonzalez M, Goldstein W, Barmada R. 2014 Factors influencing initial cup stability in total hip arthroplasty. *Clin. Biomech. (Bristol, Avon)* **29**, 1177–1185. (doi:10.1016/j.clinbiomech.2014.09.006)
91. Jette B, Brailovski V, Simoneau C, Dumas M, Terriault P. 2018 Development and *in vitro* validation of a simplified numerical model for the design of a biomimetic femoral stem. *J. Mech. Behav. Biomed. Mater.* **77**, 539–550. (doi:10.1016/j.jmbbm.2017.10.019)
92. Berahmani S, Janssen D, Wolfson D, Rivard K, de Waal Malefijt M, Verdonschot N. 2015 The effect of surface morphology on the primary fixation strength of uncemented femoral knee prosthesis: a cadaveric study. *J. Arthroplasty* **30**, 300–307. (doi:10.1016/j.arth.2014.09.030)
93. Michel A *et al*. 2017 Assessing the acetabular cup implant primary stability by impact analyses: a cadaveric study. *PLoS ONE* **11**, e0166778.
94. Branemark R *et al*. 1998 Biomechanical characterization of osseointegration: an experimental *in vivo* investigation in the beagle dog. *J. Orthop. Res.* **16**, 61–69. (doi:10.1002/jor.1100160111)
95. Shirazi-Adl A. 1992 Finite element stress analysis of a push-out test. Part 1: Fixed interface using stress compatible elements. *J. Biomech. Eng.* **114**, 111–118. (doi:10.1115/1.2895434)
96. Nguyen VH *et al*. 2017 Influence of anisotropic bone properties on the biomechanical behavior of the acetabular cup implant: a multiscale finite element study. *Comput. Methods Biomech. Biomed. Engin.* **20**, 1312–1325. (doi:10.1080/10255842.2017.1357703)
97. Raffa ML *et al*. Submitted. Dependence of the primary stability of acetabular cup implants on its biomechanical environment. *Proc. Inst. Mech. Eng. H*.
98. Rancourt D, Shirazi-Adl A, Drouin G, Paiement G. 1990 Friction properties of the interface between porous-surfaced metals and tibial cancellous bone. *J. Biomed. Mater. Res.* **24**, 1503–1519. (doi:10.1002/jbm.820241107)
99. Jäger J. 1995 Axi-symmetric bodies of equal material in contact under torsion or shift. *Arch. Appl. Mech.* **65**, 478–487. (doi:10.1007/BF00835661)
100. Dammak M, Shirazi-Adl A, Schwartz M, Gustavson L. 1997 Friction properties at the bone-metal interface: comparison of four different porous metal surfaces. *J. Biomed. Mater. Res.* **35**, 329–336. (doi:10.1002/(SICI)1097-4636(19970605)35:3<329::AID-JBM7>3.0.CO;2-J)
101. Grant JA, Bishop N, Sprecher C, Honl M, Morlock MM. 2007 Artificial composite bone as a model of human trabecular bone: the implant-bone interface. *J. Biomech.* **40**, 1158–1164. (doi:10.1016/j.jbiomech.2006.04.007)
102. Spears IR, Pfleiderer M, Schneider E, Hille E, Morlock MM. 2001 The effect of interfacial parameters on cup-bone relative micromotions. A finite element investigation. *J. Biomech.* **34**, 113–120. (doi:10.1016/S0021-9290(00)00112-3)
103. Michel A, Nguyen V-H, Bosc R, Vayron R, Hernigou P, Naili S, Haiat G. 2017 Finite element model of the impaction of a press-fitted acetabular cup. *Med. Biol. Eng. Comput.* **55**, 781–791. (doi:10.1007/s11517-016-1545-2)
104. Damm NB, Morlock MM, Bishop NE. 2015 Friction coefficient and effective interference at the implant-bone interface. *J. Biomech.* **48**, 3517–3521. (doi:10.1016/j.jbiomech.2015.07.012)
105. Bishop NE, Rothstock S, Damm NB, Morlock MM. 2014 The influence of bone damage on press-fit mechanics. *J. Biomech.* **47**, 1472–1478. (doi:10.1016/j.jbiomech.2014.01.029)
106. Damm NB, Morlock MM, Bishop NE. 2017 Influence of trabecular bone quality and implantation direction on press-fit mechanics. *J. Orthop. Res.*, **35**, 224–233. (doi:10.1002/jor.23257)
107. Zhang Y, Ahn PB, Fitzpatrick DC, Heiner AD, Poggie RA, Brown TD. 1999 Interfacial frictional behavior: cancellous bone, cortical bone, and a novel porous tantalum biomaterial. *J. Musculoskelet. Res.* **3**, 245–251. (doi:10.1142/S0218957799000269)
108. Castellani C, Lindtner RA, Hausbrandt P, Tschegg E, Stanzl-Tschegg SE, Zanoni G, Beck S, Weinberg A-M. 2011 Bone-implant interface strength and osseointegration: biodegradable magnesium alloy versus standard titanium control. *Acta Biomater.* **7**, 432–440. (doi:10.1016/j.actbio.2010.08.020)
109. Tschegg EK, Lindtner RA, Doblhoff-Dier V, Stanzl-Tschegg SE, Holzlechner G, Castellani C, Imwinkelried T, Weinberg A. 2011 Characterization methods of bone-implant-interfaces of bioresorbable and titanium implants by fracture mechanical means. *J. Mech. Behav. Biomed. Mater.* **4**, 766–775. (doi:10.1016/j.jmbbm.2010.08.004)
110. Nonhoff J, Moest T, Schmitt CM, Weisel T, Bauer S, Schlegel KA. 2015 Establishment of a new pull-out strength testing method to quantify early osseointegration—an experimental pilot study. *J. Craniomaxillofac. Surg.* **43**, 1966–1973. (doi:10.1016/j.jcms.2015.10.005)
111. Muller M, Hennig FF, Hothorn T, Stangl R. 2006 Bone-implant interface shear modulus and ultimate stress in a transcortical rabbit model of open-pore Ti6Al4 V implants. *J. Biomech.* **39**, 2123–2132. (doi:10.1016/j.jbiomech.2005.05.036)
112. Nakamura T, Yamamuro T, Higashi S, Kokubo T, Itoo S. 1985 A new glass-ceramic for bone replacement: evaluation of its bonding to bone tissue. *J. Biomed. Mater. Res.* **19**, 685–698. (doi:10.1002/jbm.820190608)
113. Thomas KA, Cook SD. 1985 An evaluation of variables influencing implant fixation by direct bone apposition. *J. Biomed. Mater. Res.* **19**, 875–901. (doi:10.1002/jbm.820190802)
114. Ronold HJ, Ellingsen JE. 2002 The use of a coin shaped implant for direct *in situ* measurement of attachment strength for osseointegrating biomaterial surfaces. *Biomaterials* **23**, 2201–2209. (doi:10.1016/S0142-9612(01)00353-2)
115. Gross U, Brandes J, Strunz V, Bab I, Sela J. 1981 The ultrastructure of the interface between a glass ceramic and bone. *J. Biomed. Mater. Res.* **15**, 291–305. (doi:10.1002/jbm.820150302)
116. Coelho PG, Zavanelli RA, Salles MB, Yeniyol S, Tovar N, Jimbo R. 2016 Enhanced bone bonding to nanotextured implant surfaces at a short healing period: a biomechanical tensile testing in the rat

femur. *Implant Dent.* **25**, 322–327. (doi:10.1097/ID.0000000000000436)

117. Mathieu V, Vayron R, Barthel E, Dalmas D, Soffer E, Anagnostou F, Haiat G. 2012 Mode III cleavage of a coin-shaped titanium implant in bone: effect of friction and crack propagation. *J. Mech. Behav. Biomed. Mater.* **8**, 194–203. (doi:10.1016/j.jmbbm.2011.12.012)
118. Ronold HJ, Lyngstadaas SP, Ellingsen JE. 2003 Analysing the optimal value for titanium implant roughness in bone attachment using a tensile test. *Biomaterials* **24**, 4559–4564. (doi:10.1016/S0142-9612(03)00256-4)
119. Ronold HJ, Ellingsen JE, Lyngstadaas SP. 2003 Tensile force testing of optimized coin-shaped titanium implant attachment kinetics in the rabbit tibiae. *J. Mater. Sci. Mater. Med.* **14**, 843–849. (doi:10.1023/A:1025622407727)
120. Ronold HJ, Lyngstadaas SP, Ellingsen JE. 2003 A study on the effect of dual blasting with TiO_2 on titanium implant surfaces on functional attachment in bone. *J. Biomed. Mater. Res. A* **67**, 524–530. (doi:10.1002/jbm.a.10580)
121. Svehla M, Morberg P, Zicat B, Bruce W, Sonnabend D, Walsh WR. 2000 Morphometric and mechanical evaluation of titanium implant integration: comparison of five surface structures. *J. Biomed. Mater. Res.* **51**, 15–22. (doi:10.1002/(SICI)1097-4636(200007)51:1<15::AID-JBM3>3.0.CO;2-9)
122. Maugis D. 2000 Frictionless elastic contact. In *Contact adhesion and rupture of elastic solids*, p. 236. Berlin, Germany: Springer.
123. Johansson CB, Jimbo R, Stefenson P. 2012 *Ex vivo* and *in vivo* biomechanical test of implant attachment to various materials: introduction of a new user-friendly removal torque equipment. *Clin. Implant Dent. Relat. Res.* **14**, 603–611. (doi:10.1111/j.1708-8208.2010.00296.x)
124. Chateauminois A, Fretigny C, Olanier L. 2010 Friction and shear fracture of an adhesive contact under torsion. *Phys. Rev. E Stat. Nonlin. Soft Matter Phys.* **81**(2 Pt 2), 026106. (doi:10.1103/PhysRevE.81.026106)
125. Franchi M, Bacchelli B, Giavaresi G, De Pasquale V, Martini D, Fini M, Giardino R, Ruggeri A. 2007 Influence of different implant surfaces on peri-implant osteogenesis: histomorphometric analysis in sheep. *J. Periodontol.* **78**, 879–888. (doi:10.1902/jop.2007.060280)
126. Mukherjee K, Gupta S. 2016 Bone ingrowth around porous-coated acetabular implant: a three-dimensional finite element study using mechanoregulatory algorithm. *Biomech. Model. Mechanobiol.* **15**, 389–403. (doi:10.1007/s10237-015-0696-7)
127. Ascenzi MG, Kawas NP, Lutz A, Kardas D, Nackenhorst U, Keyak JH. 2013 Individual-specific multi-scale finite element simulation of cortical bone of human proximal femur. *J. Comput. Phys.* **244**, 298–311. (doi:10.1016/j.jcp.2012.05.027)
128. Nackenhorst U, Lenz C. 2005 Biomechanics of bones on various length scales. *Proc. Appl. Math. Mech.* **5**, 31–34. (doi:10.1002/pamm.200510009)
129. Nackenhorst U. 2006 Computational methods for studies on the biomechanics of bones. *Found. Civ. Environ. Eng.* **7**, 251–271.
130. Abdel-Wahab A, Silberschmidt V. 2013 Plastic behaviour of microstructural constituents of cortical bone tissue: a nanoindentation study. *Int. J. Exp. Comput. Biomech.* **2**, 136–157. (doi:10.1504/IJECB.2013.056521)
131. Demiral M, Abdel-Wahab A, Silberschmidt V. 2015 A numerical study on indentation properties of cortical bone tissue: influence of anisotropy. *Acta Bioeng. Biomech.* **17**, 3–14.
132. Anchieta RB, Baldassarri M, Guastaldi F, Tovar N, Janal MN, Gottlow J, Dard M, Jimbo R, Coelho PG. 2014 Mechanical property assessment of bone healing around a titanium-zirconium alloy dental implant. *Clin. Implant Dent. Relat. Res.* **16**, 913–919. (doi:10.1111/cid.12061)
133. Jandt KD. 2001 Atomic force microscopy of biomaterials surfaces and interfaces. *Surf. Sci.* **491**, 303–332. (doi:10.1016/S0039-6028(01)01296-1)
134. Clark PA, Clark AM, Rodriguez A, Hussain MA, Mao JJ. 2007 Nanoscale characterization of bone–implant interface and biomechanical modulation of bone ingrowth. *Mater. Sci. Eng. C Mater. Biol. Appl.* **27**, 382–393. (doi:10.1016/j.msec.2006.05.056)
135. Chang MC, Ko CC, Liu CC, Douglas WH, DeLong R, Seong W-J, Hodges J, An K-N. 2003 Elasticity of alveolar bone near dental implant-bone interfaces after one month's healing. *J. Biomech.* **36**, 1209–1214. (doi:10.1016/S0021-9290(03)00113-1)
136. Vayron R, Barthel E, Mathieu V, Soffer E, Anagnostou F, Haiat G. 2012 Nanoindentation measurements of biomechanical properties in mature and newly formed bone tissue surrounding an implant. *J. Biomech. Eng.* **134**, 021007. (doi:10.1115/1.4005981)
137. Vayron R, Matsukawa M, Tsubota R, Mathieu V, Barthel E, Haiat G. 2014 Evolution of bone biomechanical properties at the micrometer scale around titanium implant as a function of healing time. *Phys. Med. Biol.* **59**, 1389–1406. (doi:10.1088/0031-9155/59/6/1389)
138. Vayron R, Barthel E, Mathieu V, Soffer E, Anagnostou F, Haiat G. 2011 Variation of biomechanical properties of newly formed bone tissue determined by nanoindentation as a function of healing time. *Comput. Methods Biomech. Biomed. Engin.* **14**(Suppl 1), 139–140. (doi:10.1080/10255842.2011.593770)
139. Tai K, Dao M, Suresh S, Palazoglu A, Ortiz C. 2007 Nanoscale heterogeneity promotes energy dissipation in bone. *Nat. Mater.* **6**, 454–462. (doi:10.1038/nmat1911)
140. Wenger MP, Bozec L, Horton MA, Mesquida P. 2007 Mechanical properties of collagen fibrils. *Biophys. J.* **93**, 1255–1263. (doi:10.1529/biophysj.106.103192)
141. Wennerberg A, Albrektsson T. 2009 Effects of titanium surface topography on bone integration: a systematic review. *Clin. Oral Implants Res.* **20**(Suppl. 4), S172–S184. (doi:10.1111/j.1600-0501.2009.01775.x)
142. Li L, Zhu Z, Huang C, Chen W. 2008 Ultrasound: a potential technique to improve osseointegration of dental implants. *Med. Hypotheses* **71**, 568–571. (doi:10.1016/j.mehy.2008.05.013)
143. Gluer CC, Barkmann R. 2003 Quantitative ultrasound: use in the detection of fractures and in the assessment of bone composition. *Curr. Osteoporos. Rep.* **1**, 98–104. (doi:10.1007/s11914-996-0003-8)
144. Vayron R, Nguyen V-H, Bosc R, Naili S. 2016 Assessment of the biomechanical stability of a dental implant with quantitative ultrasound: a three-dimensional finite element study. *J. Acoust. Soc. Am.* **139**, 773–780. (doi:10.1121/1.4941452)
145. Vayron R, Nguyen V-H, Bosc R, Naili S. 2015 Finite element simulation of ultrasonic wave propagation in a dental implant for biomechanical stability assessment. *Biomech. Model. Mechanobiol.* **14**, 1021–1032. (doi:10.1007/s10237-015-0651-7)
146. Heriveaux Y, Nguyen VH, Haiat G. 2018 Reflection of an ultrasonic wave on the bone-implant interface: a numerical study of the effect of the multiscale roughness. *J. Acoust. Soc. Am.* **144**, 488. (doi:10.1121/1.5046524)
147. Zahn D, Duchstein P. 2016 Multi-scale modelling of deformation and fracture in a biomimetic apatite-protein composite: molecular-scale processes lead to resilience at the μm-scale. *PLoS ONE* **11**, e0157241.
148. Palmquist A. 2018 A multiscale analytical approach to evaluate osseointegration. *J. Mater. Sci. Mater. Med.* **29**, 60. (doi:10.1007/s10856-018-6068-y)
149. Du J, Lee J-H, Jang AT, Gu A, Hossaini-Zadeh M, Prevost R, Curtis DA, Ho SP. 2015 Biomechanics and strain mapping in bone as related to immediately-loaded dental implants. *J. Biomech.* **48**, 3486–3494. (doi:10.1016/j.jbiomech.2015.05.014)
150. Thorfve A, Palmquist A, Grandfield K. 2015 Three-dimensional analytical techniques for evaluation of osseointegrated titanium implants. *Mater. Sci. Technol.* **31**, 174–179. (doi:10.1179/1743284714Y.0000000687)
151. Mao Q, Su K, Zhou Y, Zadeh MH, Lewis GS, Du J. 2019 Voxel-based micro-finite element analysis of dental implants in a human cadaveric mandible: tissue modulus assignment and sensitivity analyses. *J. Mech. Behav. Biomed. Mater.* **94**, 229–237. (doi:10.1016/j.jmbbm.2019.03.008)
152. Hirata K, Kubota T, Koyama D, Takayanagi S, Matsukawa M. 2017 Fabrication of oriented hydroxyapatite film by RF magnetron sputtering. *AIP Adv.* **7**, 085219. (doi:10.1063/1.5000490)
153. Nakano T, Kaibara K, Tabata Y, Nagata N, Enomoto S, Marukawa E, Umakoshi Y. 2002 Unique alignment and texture of biological apatite crystallites in typical calcified tissues analyzed by microbeam X-ray diffractometer system. *Bone* **31**, 479–487. (doi:10.1016/S8756-3282(02)00850-5)
154. Yamato Y, Matsukawa M, Yanagitani T, Yamazaki K, Mizukawa H, Nagano A. 2008 Correlation between hydroxyapatite crystallite orientation and ultrasonic

wave velocities in bovine cortical bone. *Calcif. Tissue Int.* **82**, 162–169. (doi:10.1007/s00223-008-9103-z)

155. Ishimoto T, Nakano T, Umakoshi Y, Tabata Y. 2009 Changes in bone microstructure and toughness during the healing process of long bones. *J. Phys. Conf. Ser.* **165**, 012085. (doi:10.1088/1742-6596/165/1/012085)
156. Ishimoto T, Nakano T, Umakoshi Y, Yamamoto M, Tabata Y. 2013 Degree of biological apatite c-axis orientation rather than bone mineral density controls mechanical function in bone regenerated using recombinant bone morphogenetic protein-2. *J. Bone Miner. Res.* **28**, 1170–1179. (doi:10.1002/jbmr.1825)
157. Matsugaki A, Isobe Y, Saku T, Nakano T. 2015 Quantitative regulation of bone-mimetic, oriented collagen/apatite matrix structure depends on the degree of osteoblast alignment on oriented collagen substrates. *J. Biomed. Mater. Res. A* **103**, 489–499. (doi:10.1002/jbm.a.35189)
158. Bunger MH, Foss M, Erlacher K, Li H, Zou X, Langdahl BL, Birkedal H, Besenbacher F, Pedersen JS. 2006 Bone nanostructure near titanium and porous tantalum implants studied by scanning small angle x-ray scattering. *Eur. Cell. Mater.* **12**, 81–91. (doi:10.22203/eCM.v012a10)
159. Ziv V, Wagner HD, Weiner S. 1996 Microstructure-microhardness relations in parallel-fibered and lamellar bone. *Bone* **18**, 417–428. (doi:10.1016/8756-3282(96)00049-X)
160. Noyama Y, Ishimoto T, Kuramoto K, Sakai T, Yoshikawa H, Nakano T. 2010 Quantity and quality of regenerated bone in grooves aligned at different angles from the implant surface. *Mater. Sci. Forum.* **654**, 2241–2244.
161. Kuroshima S, Nakano T, Ishimoto T, Sasaki M, Inoue M, Yasutake M, Sawase T. 2017 Optimally oriented grooves on dental implants improve bone quality around implants under repetitive mechanical loading. *Acta Biomater.* **48**, 433–444. (doi:10.1016/j.actbio.2016.11.021)
162. Selvik G. 1989 Roentgen stereophotogrammetry: a method for the study of the kinematics of the skeletal system. *Acta Orthop. Scand.* **60**, 1–51. (doi:10.3109/17453678909154184)
163. Kärrholm J. 1989 Roentgen stereophotogrammetry: review of orthopedic applications. *Acta Orthop. Scand.* **60**, 491–503. (doi:10.3109/17453678909149328)
164. Valstar ER, Gill R, Ryd L, Flivik G. 2005 Guidelines for standardization of radiostereometry (RSA) of implants. *Acta Orthop.* **76**, 563–572. (doi:10.1080/17453670510041574)
165. Soballe K, Toksvig-Larsen S, Gelineck J, Fruensgaard S, Hansen ES, Ryd L, Lucht U, Bunger C. 1993 Migration of hydroxyapatite coated femoral prostheses. A Roentgen Stereophotogrammetric study. *J. Bone Joint Surg. Br.* **75**, 681–687. (doi:10.1302/0301-620X.75B5.8397213)
166. Isaksson H, Le Cann S, Perdikouri C, Turunen MJ, Kaestner A, Hall SA, Tudisco E. 2017 Neutron tomographic imaging of bone-implant interface: comparison with X-ray tomography. *Bone* **103**, 295–301. (doi:10.1016/j.bone.2017.07.022)
167. Le Cann S, Tudisco E, Perdikouri C, Belfrage O, Kaestner A, Hall S, Isaksson H. 2017 Characterization of the bone-metal implant interface by digital volume correlation of *in-situ* loading using neutron tomography. *J. Mech. Behav. Biomed. Mater.* **75**, 271–278. (doi:10.1016/j.jmbbm.2017.07.001)
168. Grandfield K, Mcnally EA, Palmquist A, Botton GA, Thomsen P, Engqvist H. 2010 Visualizing biointerfaces in three dimensions: electron tomography of the bone-hydroxyapatite interface. *J. R. Soc. Interface* **7**, 1497–1501. (doi:10.1098/rsif.2010.0213)
169. Grandfield K, Gustafsson S, Palmquist A. 2013 Where bone meets implant: the characterization of nano-osseointegration. *Nanoscale* **5**, 4302–4308. (doi:10.1039/c3nr00826f)
170. Sroka-Bartnicka A *et al.* 2015 The biocompatibility of carbon hydroxyapatite/beta-glucan composite for bone tissue engineering studied with Raman and FTIR spectroscopic imaging. *Anal. Bioanal. Chem.* **407**, 7775–7785. (doi:10.1007/s00216-015-8943-4)
171. Gourion-Arsiquaud S, Marcott C, Hu Q, Boskey AL. 2014 Studying variations in bone composition at nano-scale resolution: a preliminary report. *Calcif. Tissue Int.* **95**, 413–418. (doi:10.1007/s00223-014-9909-9)
172. Mandair GS, Morris MD. 2015 Contributions of Raman spectroscopy to the understanding of bone strength. *Bonekey Rep.* **4**, 620. (doi:10.1038/bonekey.2014.115)
173. Raghavan M, Sahar ND, Kohn DH, Morris MD. 2012 Age-specific profiles of tissue-level composition and mechanical properties in murine cortical bone. *Bone* **50**, 942–953. (doi:10.1016/j.bone.2011.12.026)
174. Shah FA, Snis A, Matic A, Thomsen P, Palmquist A. 2016 3D printed Ti6Al4 V implant surface promotes bone maturation and retains a higher density of less aged osteocytes at the bone-implant interface. *Acta Biomater.* **30**, 357–367. (doi:10.1016/j.actbio.2015.11.013)
175. Krishna BV, Bose S, Bandyopadhyay A. 2007 Low stiffness porous Ti structures for load-bearing implants. *Acta Biomater.* **3**, 997–1006. (doi:10.1016/j.actbio.2007.03.008)
176. Korabi R, Shemtov-Yona K, Rittel D. 2017 On stress/strain shielding and the material stiffness paradigm for dental implants. *Clin. Implant Dent. Relat. Res.* **19**, 935–943. (doi:10.1111/cid.12509)
177. Korabi R, Shemtov-Yona K, Dorogoy A, Rittel D. 2017 The failure envelope concept applied to the bone-dental implant system. *Sci. Rep.* **7**, 2051. (doi:10.1038/s41598-017-02282-2)
178. Craven TG, Carson WL, Asher MA, Robinson RG. 1994 The effects of implant stiffness on the bypassed bone mineral density and facet fusion stiffness of the canine spine. *Spine (Phila Pa 1976)* **19**, 1664–1673. (doi:10.1097/00007632-199408000-00003)
179. Simon U, Augat P, Ignatius A, Claes L. 2003 Influence of the stiffness of bone defect implants on the mechanical conditions at the interface—a finite element analysis with contact. *J. Biomech.* **36**, 1079–1086. (doi:10.1016/S0021-9290(03)00114-3)
180. Stoppie N, Van Oosterwyck H, Jansen J, Wolke J, Wevers M, Naert I. 2009 The influence of Young's modulus of loaded implants on bone remodeling: an experimental and numerical study in the goat knee. *J. Biomed. Mater. Res. A* **90**, 792–803. (doi:10.1002/jbm.a.32145)
181. Gottlow J, Dard M, Kjellson F, Obrecht M, Sennerby L. 2012 Evaluation of a new titanium-zirconium dental implant: a biomechanical and histological comparative study in the mini pig. *Clin. Implant Dent. Relat. Res.* **14**, 538–545. (doi:10.1111/j.1708-8208.2010.00289.x)
182. Arabnejad S, Johnston B, Tanzer M, Pasini D. 2017 Fully porous 3D printed titanium femoral stem to reduce stress-shielding following total hip arthroplasty. *J. Orthop. Res.* **35**, 1774–1783. (doi:10.1002/jor.23445)
183. Lin DJ, Chuang C-C, Chern Lin J-H, Lee J-W, Ju C-P, Yin H-S. 2007 Bone formation at the surface of low modulus Ti–7.5Mo implants in rabbit femur. *Biomaterials* **28**, 2582–2589. (doi:10.1016/j.biomaterials.2007.02.005)
184. Sumitomo N, Noritake K, Hattori T, Morikawa K, Niwa S, Sato K, Niinomi M. 2008 Experiment study on fracture fixation with low rigidity titanium alloy: plate fixation of tibia fracture model in rabbit. *J. Mater. Sci. Mater. Med.* **19**, 1581–1586. (doi:10.1007/s10856-008-3372-y)
185. Shi L *et al.* 2013 The improved biological performance of a novel low elastic modulus implant. *PLoS ONE* **8**, e55015. (doi:10.1371/journal.pone.0055015)
186. Kasemo B, Gold J. 1999 Implant surfaces and interface processes. *Adv. Dent. Res.* **13**, 8–20. (doi:10.1177/08959374990130011901)
187. Le Guehennec L, Soueidan A, Layrolle P, Amouriq Y. 2007 Surface treatments of titanium dental implants for rapid osseointegration. *Dent. Mater.* **23**, 844–854. (doi:10.1016/j.dental.2006.06.025)
188. Wennerberg A, Albrektsson T. 2010 On implant surfaces: a review of current knowledge and opinions. *Int. J. Oral Maxillofac. Implants* **25**, 63–74.
189. Wennerberg A, Albrektsson T. 2000 Suggested guidelines for the topographic evaluation of implant surfaces. *Int. J. Oral Maxillofac. Implants* **15**, 331–344.